# Estimating DBH with iPad Pro LiDAR in Boreal Forests: Methodological considerations and a case study in natural boreal forests

by

Matthew Guenther

B.Sc. Forestry (Honors), Lakehead University, 2022

A Thesis, Dissertation, or Report Submitted in Partial Fulfillment

of the Requirements for the Degree of

**M.Sc. Forestry**

in the Graduate Academic Unit of Natural Resources Management

Supervisory Committee: Muditha H. Heenkenda, Ph.D.,
Brigitte Leblon, Ph.D.,
Dave M. Morris, Ph.D.

Examining Committee: Muditha H. Heenkenda, Ph.D.,
Brigitte Leblon, Ph.D.,
Dave M. Morris, Ph.D.,
Ulf Runesson, Ph. D. (External Examiner)

This thesis is accepted by the

Dean of Graduate Studies

LAKEHEAD UNIVERSITY

April 2024

## ABSTRACT

Diameter at Breast Height (DBH) is the measure of the diameter of a tree stem 1.3 meters above the ground. DBH is a key variable measured in Forest Resource Inventories (FRIs) and is traditionally measured manually, which is labour-intensive. The 2020 Apple iPad Pro 12th Generation is a lightweight, consumer-level tablet with an integrated LiDAR scanner with a maximum range of 5 m and a positional accuracy of ±1 cm. The overall objective was to examine the feasibility of estimating DBH in boreal forests with iPad Pro LiDAR. A scoping study was conducted in a plantation forest (48.37°N, 89.39°W) near Thunder Bay, ON, Canada, with the specific objective of determining an optimal method for DBH estimation with the iPad Pro. Different combinations of scanning methods (i.e., circular, figure-8, transect), numbers of stem cross-sections (i.e., one or five), sizes of stem cross-sections (i.e., 4 or 10 cm), and curve-fitting formulas (i.e., Pratt's circle fit, Taubin's circle fit, Taubin's ellipse fit, Szpak's ellipse fit) were tested to identify the combination producing the most accurate estimates of DBH. The optimal method was the circular scanning pattern with a single 4 cm cross-section and a combination of circle- and ellipse-fitting formulas (RMSE = 1.1 cm; 6.2%). The second specific objective was to determine the accuracy of DBH values estimated with the optimal method in natural boreal forests. DBH was estimated for 133 trees on 15 sites in northern Ontario, Canada, representing a range of natural boreal forest site conditions. A secondary objective was to determine if the tested stand- (i.e., species composition, age, density, understory density) or tree-level attributes (i.e., species, actual DBH) significantly impacted the accuracy of estimated DBH values. An RMSE of 1.5 cm (8.6%) was achieved. Estimated DBH was within 1 cm of actual DBH for 78 of 133 (59%) measured trees. Stand age had a large effect (> 0.15) on the accuracy of estimated DBH values, while density, understory density, and actual DBH had moderate effects (0.05-0.15). In both studies, Inertial Measurement Unit (IMU) and positional accuracy errors with the iPad Pro LiDAR scanner limited the accuracy of DBH estimates. Future studies should incorporate a greater number of natural boreal forest sites to better understand the impacts of different stand and tree attributes on the accuracy of estimated DBH values. Future studies should also compare the accuracy of DBH values estimated from the iPad Pro and those estimated from traditional MLS and TLS for the same sites to identify the trade-off between device cost, device size, and accuracy. However, the scanning range of the device limits the variables that can be estimated from LiDAR data, rendering it unsuitable for use in FRIs until the scanning range is improved.

## ACKNOWLEDGEMENTS

I would like to thank my advisory committee: Dr. Muditha K. Heenkenda, Dr. Brigitte Leblon, and Dr. Dave M. Morris for their guidance, assistance, and willingness to help. I would also like to thank the Center for Northern Forest Ecosystem Research (CNFER), Ontario Forest Resource Inventory Unit (FRIu), and the OMNRF as a whole for their support in designing and conducting the fieldwork for this project. Special thanks go to Georgie Robere-McGugan (FRIu) and Dr. Dave M. Morris (CNFER) for arranging the partnership with the OMNRF for this project; Kyle Webb (CNFER) for his assistance planning and conducting fieldwork; and, Domenic McVey and Josh Oleksuk (CNFER) for their assistance conducting fieldwork.

The completion of this thesis would not have been possible without funding support from Dr. Muditha H. Heenkenda (Research Development Grant, LU); the Faculty of Natural Resources Management at Lakehead University (Graduate Assistantship); and, the Ontario Ministry of Natural Resources (Paid Summer Internship).

## TABLE OF CONTENTS

## LIST OF TABLES

## LIST OF FIGURES

# CHAPTER 1: INTRODUCTION

Diameter at Breast Height (DBH) is the measure of a tree stem 1.3 m above the ground, and is considered a key attribute that is measured in Forest Resource Inventories (FRIs) (Chiappini et al. 2022). DBH is traditionally measured using implements such as diameter tape or callipers, which are time-consuming and thus expensive (Aijazi et al. 2017). As FRIs have evolved alongside forest management policy and legislation, the quantity and depth of information measured in FRIs have increased (Bilyk et al. 2021). Data summarized in FRIs represent the foundational information used to guide forest management planning and implementation, as well as helping to understand changes in forest landscapes over time (White et al. 2016). As a result, accurate and timely FRIs are essential to monitor complex and dynamic landscapes. In addition to DBH, FRIs also measure or calculate (based on field measurements) other variables such as soil conditions, stand understory vegetation species composition, stem density, and stand volume (OMNRF 2015). In Ontario, this is done to determine the suitability of a site for harvest and to identify specific methods of harvesting and regeneration best-suited for the site (OMNRF 2015).

Since the advent of Light Detection and Ranging (LiDAR) technologies, numerous studies have investigated different methods of using LiDAR to measure forest parameters (Blanco et al. 2015; Côté et al. 2011; Lovell et al. 2003; Woods et al. 2011). Airborne Laser Scanning (ALS) from manned aircrafts and ALS from Unmanned Aerial Vehicles (UAVs) are recognized as more efficient than terrestrial systems in terms of time required to create dense point clouds (Brede et al. 2017). However, unlike terrestrial systems, ALS cannot provide below-canopy stem profiles with a high enough point density to allow estimation of DBH (Woods et al. 2011; Dassot et al. 2011; Hyyppä et al. 2011). UAV LiDAR addresses many of the problems with ALS by capturing a high density of points in a versatile, customizable platform that can be flown above or below

canopy, albeit with lower point densities than most Terrestrial Laser Scanning (TLS) systems (Brede et al. 2017). Therefore, TLS may be best suited for estimating DBH. TLS was first used for forest inventory by Hopkinson et al. (2004), who accurately measured or derived stem location, tree heights, DBH, site density, and timber volume from point cloud data. Bauwens et al. (2016) used TLS to accurately estimate other forest inventory metrics, including basal area, gap fraction, and Leaf Area Index (LAI), and confirmed that it is more time efficient than manual measurements. A key finding for accurate estimation of DBH from LiDAR data have been the necessity to capture tree stems from multiple perspectives due to the irregular shapes of tree stems (Pfeifer and Winterhalder 2004; Hunčaga et al. 2020). Other studies have shown the use of least-squares curve-fitting formulas (circle- and ellipse-fit) to produce highly accurate estimates of DBH (Wang et al. 2021; Tatsumi et al. 2021; Gülci et al. 2023).

Tree stem cross-sections were first modelled by Pfeifer and Winterhalder (2004), who used free-form *b*-spline formulas with mean square error to fit irregular curves to point cloud data. Later, Hopkinson et al. (2004) estimated DBH with a least-squares regression cylinder fit, applied to a single three-dimensional cross-section of each stem 1.25-1.75 m above ground. Pfeifer and Winterhalder (2004) and other more recent studies have suggested that point cloud data should be acquired from multiple perspectives and capture much of the tree stem for accurate cross-section modelling due to tree stems' irregular, uneven shapes (Hunčaga et al. 2020; Wang et al. 2022). Recently, Liang et al. (2018) found in a benchmarking study that using multiple scans of a forest plot significantly improved the accuracy of forest metrics estimated from TLS data. Despite the high accuracy of DBH estimations derived from TLS reported in recent studies, several factors, including device costs, have prevented these systems from being widely integrated in forest inventories (Calders et al. 2020; Luetzenburg et al. 2011).

Since the advent of the first terrestrial LiDAR scanners, device weight and size have decreased while maintaining a high accuracy of DBH estimates from acquired point cloud data (Liu et al. 2018). Modern Mobile Laser Scanners (MLS) weigh less than 1 kg, although these devices often lack durability for continuous use in remote forest environments (Liu et al. 2018).

In 2020, Apple released the iPad Pro 4th Generation, a consumer tablet with an integrated single-photon receptor LiDAR scanner with a maximum scanning range of 5m and a point accuracy of ±1 cm (Apple 2020; Gollob et al. 2021). If this device can be used to reliably estimate forest attributes common in forest inventories, such as stem location, DBH, or basal area, this would offer an improvement in efficiency and a reduction in operating costs for the undertaker of the inventory, relative to TLS or manual measurements. As shown in Table 1.1, this device has been used to estimate DBH in natural, urban and plantation forests with an accuracy that varies between 10.30% (rRMSE) and 27.00% (rRMSE).

**Table 1.1.** RMSE (cm) and rRMSE (%) values recorded in previous studies that used an iPad Pro LiDAR scanner to estimate DBH.

| RMSE (cm) | rRSME (%) | Curve-Fitting Method | Forest Type | Location | Species | Authors |
|---|---|---|---|---|---|---|
| 2.78 | 7.00 | Circle Fit | Urban Park | Zvolen, Slovakia | N/A | Wang et al. (2021) |
| 2.30 | 10.50 | Circle Fit | Natural and Plantation | Hokkaido, Japan | Coniferous and Deciduous | Tatsumi et al. (2021) |
| 3.13 | 10.50 | Ellipse Fit | Research Forest | Forchtenstein, Austria | Coniferous and Deciduous | Gollob et al. (2021) |
| 2.70 | 10.80 | RANSAC Algorithm | Plantation | Cesane Forest, Italy | *Pinus nigra* J.F. Arnold and *Fraxinus ornus* L. | Chiappini et al. (2022) |
| 2.33 | 11.66 | Circle Fit | University Campus | Kahramanmaraş, Türkiye | *Pinus brutia* Ten. and *Platanus orientalis* L. | Gülci et al. (2023) |
| 2.82 | 12.82 | Manual | Plantation | Thunder Bay, Canada | *Pinus resinosa* | Wang et al. (2022) |
| 5.18 | 13.03 | Circle Fit | Urban Park | Zvolen, Slovakia | N/A | Wang et al. (2021) |
| 4.10 | 16.30 | Circle Fit | Plantation | Cesane Forest, Italy | *Pinus nigra* and *Fraxinus ornus* | Chiappini et al. (2022) |
| 6.29 | 21.23 | Cylinder Fit | Research Forest | Forchtenstein, Austria | Coniferous and Deciduous | Gollob et al. (2020) |
| 5.90 | 26.82 | Manual | Plantation | Thunder Bay, Canada | *Pinus resinosa* | Wang et al. (2022) |
| 6.80 | 27.00 | Voxelization | Plantation | Cesane Forest, Italy | *Pinus nigra* and *Fraxinus ornus* | Chiappini et al. (2022) |

Despite previous studies demonstrating that LiDAR can be used to accurately estimate DBH, LiDAR has not replaced manual methods of DBH mensuration in most forest inventories due to several factors, such as high device costs (Calders et al. 2020; Luetzenburg et al. 2021).

In 2020, Apple (Cupertino, CA, USA) released the 12th Generation iPad Pro, a consumer tablet with an integrated single-photon receptor LiDAR scanner, with a scanning range up to 5 m and a positional accuracy (for points in acquired point clouds) of ±1cm (Apple 2020; Gollob et al. 2021). Several studies have tested this device for DBH estimation in a range of forest environments, such as plantation, urban, or natural forests (Chiappini et al. 2022; Wang et al. 2021; Tatsumi et al. 2021; Gülci et al. 2023; Gollob et al. 2021; Wang et al. 2022). However, the point cloud acquisition and processing methods, as well as the methods of extracting DBH from the acquired point clouds, vary between these previous studies. As the studies took place in a range of environments, direct comparisons of results to identify an optimal method for DBH estimation with iPad Pro LiDAR are not readily available. Additionally, no studies to date have compared different methods of acquisition, processing, and DBH estimation concurrently on a single site.

As Table 1.1 shows, studies have taken place in urban and plantation forests in various forest regions. Differences in accuracies between these studies stem from the use of different scanning applications used to acquire point cloud data, different methods of scanning visited sites (Individual trees, static whole site, mobile scanning), the use of different software and tools to process point clouds to estimate DBH, different site conditions (Slope, understory vegetation), and different species of tree with varying conditions of bark being scanned. These studies mainly scanned multiple trees at once while moving, identified ground features to locate breast height, and applied a curve-fitting algorithm to a stem cross-section to estimate DBH. While circle-fitting algorithms were most commonly used and produced the most accurate results, the accuracy of ellipse-fitting formulas demonstrated by Gollob et al. (2021) suggests additional investigation is worthwhile.

Among already tested TLS scanning patterns- circular (Figure 1.1a), figure-8 (Figure 1.1b;), and transect (Figure 1.1c) provided promising results. For example, the

circular pattern was implemented for DBH estimation using the iPad Pro 12th Generation and a ZEB HORIZON Personal Laser Scanner (PLS) and achieved considerable accuracy (Gollob et al. 2021).

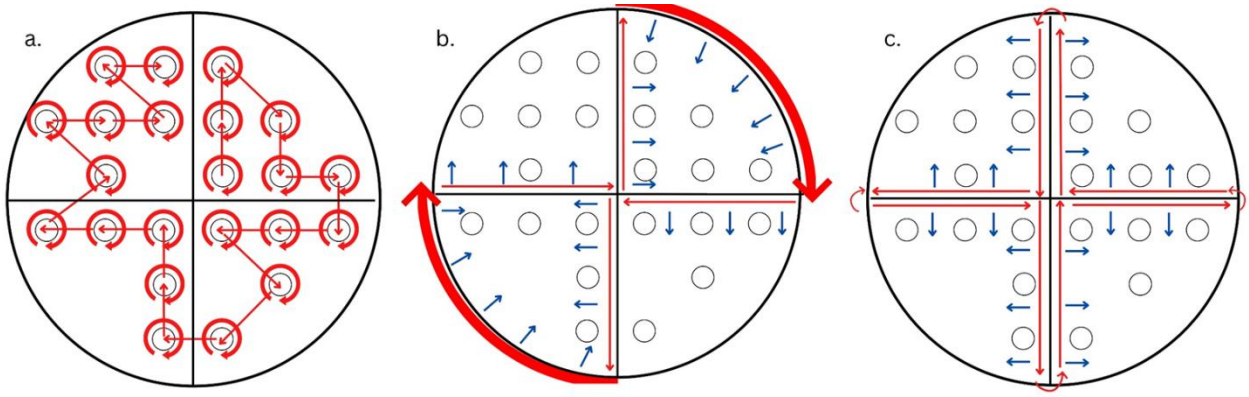


**Figure 1.1.** Data acquisition patterns and walking paths (a) circular; (b) figure-8; and (c) transect scanning patterns. The walking path for each scanning method is displayed in red and the scanning direction is indicated with a blue arrow.

The circular scanning pattern involved walking each tree stem's circumference to create complete cross-sections of the stem (Figure 1.1 (a)). The figure-8 scanning pattern involved walking along the inside axes and half of the outside circumference of the plot, to ensure as much of each tree stem was captured as possible while prioritising the speed of acquisition (Figure 1.1(b)). The transect scanning method involved walking both axes of the plot twice, scanning perpendicularly to the plot in opposite directions each time (Figure 1.1(c)). The circular pattern prioritised detailed data, the transect method favoured acquisition speed, and the figure-8 pattern sought to balance both.

The Cloth Simulation Filtering (CSF) plugin for CloudCompare, developed by Zhang et al. (2016), can be used to identify ground features in point clouds and interpolate the ground surface for areas without data. This algorithm is commonly used to segment ground features within LiDAR datasets (Liu et al. 2018; Lee et al. 2020; Yang et al. 2020; Yu et al. 2022).

There are many different curve-fitting algorithms capable of estimating DBH, four of which were examined in this study. For 'Pratt's direct-least-squares circle fit' and 'Taubin's direct-least-squares circle fit', the points are assumed to represent a perfect circle (Chernov 2022a; Chernov 2022b; Pratt 1987; Taubin 1991). Circle-fitting algorithms have been found to produce very accurate estimates of DBH from iPad Pro LiDAR data in previous studies (Wang et al. 2021; Tatsumi et al. 2021; Gülci et al. 2023). In 'Taubin's direct-least-squares ellipse fit' and 'Szpak's ellipse fit with Sampson distance and modified Levenberg-Marquardt step', the points are assumed to represent an ellipsoid (Taubin 1991; Chernov 2022c; Szpak 2016; Szpak et al. 2015). While diameter tapes and calipers used to estimate DBH manually assume tree stems to represent perfect circles, the irregular nature of tree stems curve leads to an over-estimation of actual diameter using circles to model the tree stem (Hunčaga et al. 2020; Moran and Williams 2002). Ellipse fitting algorithms have been used to produce estimates of DBH with accuracies comparable or superior to those estimated with circle-fitting formulas (Gollob et al. 2021). The formulas developed by Pratt (1987) and Taubin (1991) are algebraic fitting formulas, which plot circles or ellipses of radius *R* around the centre point of the dataset (*a, b*) while minimizing the distance from each point in the dataset to the plotted curve; through a least-squares method (Chernov and Lesort 2005). The centre points for each fitted curve were calculated as the average X and Y values for the dataset (Pratt 1987; Taubin 1991). To solve the least-squares method, it is necessary to minimize the following non-linear Gradient-weighted Algebraic Fit (GRAF; Equation 1.1) (Chernov and Lesort 2005; Turner 1974).

$$F_4(a,b,R) = \sum_{i=1}^{n} \frac{[(x_i-a)^2+(y_i-b)^2-R^2]^2}{(x_i-a)^2+(y_i-b)^2} \qquad (1.1)$$

Where *a, b,* represent the coordinates of the centre of the fitted curve, $x$ and $y$ represent the X and Y coordinates of point $i$ in the stem shapefile, and $R$ is the radius.

The GRAF is approximated differently in Taubin's and Pratt's approaches (Chernov and Lesort 2005). In Pratt (1987), the GRAF is simplified by assuming that $(x_i - a)^2 + (y_i - b)^2 \approx R^2$ as follows (Equation 1.2):

$$F_4^i(a, b, R) = R^{-2} \sum_{i=1}^{n} [\,(x_i - a)^2 + (y_i - b)^2 - R^2]^2 \qquad (1.2)$$

In Taubin (1991), the GRAF is approximated by averaging the GRAF denominator over $1 \leqslant i \leqslant n$ (Chernov and Lesort 2004) (Equation 1.3):

$$F_4^{ii}(a, b, R) = \left(\frac{1}{\sum (x_i - a)^2 + (y_i - b)^2}\right) \text{ x } \sum_{i=1}^{n} [(x_i - a)^2 + (y_i - b)^2 - R^2]^2 \quad (1.3)$$

Pratt's approximation better handles datasets where the full circumference is not present, while Taubin's formula is seen as faster and more accurate if the full circumference is present (Chernov and Lesort 2005). Formulas 1 and 2 both fit curves to a data set of point coordinates using the least-squared method, which has previously been used to estimate DBH (Chiappini et al. 2022; Gollob et al. 2021; Wang et al. 2021; Tatsumi et al. 2021; Gülci et al. 2023).

Szpak's ellipse fit is an iterative geometric fit that uses an implicit barrier to separate feasible elliptic regions and infeasible hyperbolic regions, and uses a direct algebraic ellipse fit as the starting point (Szpak et al. 2015). The adapted Levenberg-Marquardt algorithm used by Szpak's ellipse fit searches for a solution by using the implicit barrier to guide subsequent attempts at plotting an ellipse towards the optimal solution (Szpak et al. 2015). This formula assumes any noise within the dataset (i.e., points not directly on the path of the optimal solution) follow a normal, Gaussian distribution about the optimal ellipse (Szpak et al. 2015). A disadvantage of this algorithm is that the fitting results may be depreciated ellipses or degenerated parabolas if the dataset has a large proportion of noise or is limited to a small area of the curve (Szpak et al. 2015). However, a comprehensive study which simultaneously

examines the impacts of different combinations of scanning patterns, processing methods, and curve-fitting formulas to estimate DBH is still needed.

If the iPad Pro 12th Generation LiDAR scanner can be used to accurately and efficiently estimate DBH across a broad range of natural boreal forest site conditions, undertakers of forest inventories and forest managers could benefit. The incorporation of the optimal method into forest resource inventories in place of manual mensuration of DBH would offer an increase in the efficiency of conducting forest inventories, as well as a reduction in the cost of collecting necessary data.

This thesis include two data chapters. Chapter 2 is titled: ***Estimating Tree Diameter at Breast Height (DBH) Using iPad Pro Light Detection and Ranging (LiDAR) Sensor in Boreal Forests***. The chapter summarizes a scoping study designed to compare different point cloud acquisition and processing methods developed based on existing literature to evaluate combinations of these options on the same sites directly and create an optimized workflow for the future study intended to carry out in a natural forest environment.

The results from this study has been published in *Canadian Journal of Remote Sensing*.

Guenther, M.; Heenkenda, M.K.; Leblon, B.; Morris, D.; Freeburn, J. Estimating Tree Diameter at Breast Height (DBH) Using iPad Pro LiDAR Sensor in Boreal Forests. Canadian Journal of Remote Sensing 2024, 50(1), 2295470, doi:10.1080/07038992.2023.2295470.

Chapter 3 is titled: ***Tree Diameter at Breast Height (DBH) Estimation Using an iPad Pro LiDAR Scanner: A Case Study in Boreal Forests, Ontario, Canada.*** The chapter summarizes a study designed to examine a range of natural boreal forest sites to investigate the feasibility of using the optimal methodology identified in Chapter 2 to estimate DBH in natural forest conditions.

The results from this study have been published in *Forests*.

Guenther, M.; Heenkenda, M.K.; Morris, D.; Leblon, B. Tree Diameter at Breast Height (DBH) Estimation Using an iPad Pro LiDAR Scanner: A Case Study in Boreal Forests, Ontario, Canada. Forests 2024, 15, 214, doi:10.3390/f15010214.

# CHAPTER 2: ESTIMATING TREE DIAMETER AT BREAST HEIGHT (DBH) USING IPAD PRO LIGHT DETECTION AND RANGING (LIDAR) SENSOR IN BOREAL FORESTS[1]

## 2.1. STUDY INTRODUCTION

As identified in the introduction (Chapter 1), no previous studies have comprehensively tested different combinations of point cloud acquisition and processing methods to identify the combination producing the most accurate estimates of DBH. Hence, this study is intended as a scoping study to compare different point cloud acquisition and processing methods developed based on existing literature to evaluate combinations of these options on the same sites directly and create an optimized workflow for the future study intended to carry out in a natural forest environment.

Our study expands upon Wang et al. 2022, who applied a singular, static scan and manual data processing to data acquired with an iPad Pro 12th Generation to estimate DBH in the 25th Sideroad research plantation forest near Thunder Bay, ON, Canada. The specific objectives were: (1) compare different scanning patterns with the iPad Pro for acquiring point cloud data for estimating DBH; (2) explore various data processing methods to extract DBH from the point cloud; and (3) identify the combination of acquisition and processing methods providing the most accurate estimates of DBH; and, (4) recommend a procedure for using iPad Pro LiDAR to estimate DBH.

[1] This chapter was published as Guenther, M.; Heenkenda, M.K.; Leblon, B.; Morris, D.; Freeburn, J. Estimating Tree Diameter at Breast Height (DBH) Using iPad Pro LiDAR Sensor in Boreal Forests. Canadian Journal of Remote Sensing 2024, 50(1), 2295470, doi:10.1080/07038992.2023.2295470.

## 2.2. MATERIALS AND METHODS

### 2.2.1. Study Area

The study was conducted in a research plantation forest, known as the 25th Sideroad Spacing Trial, near Thunder Bay, Ontario (48.37°N, 89.39°W) (Appendix 1). The Ontario Ministry of Natural Resources and Forestry (OMNRF) established the plantation in 1950 and has continuously managed the site (McClain et al. 1994). No stand tending operations have taken place. The trial comprises several blocks of different tree species, planted at different initial spacing distances. Three circular plots with a diameter of 10m were selected for this study, with the following characteristics: (a) Plot 'Pr', Red Pine (*Pinus resinosa*) with 1.8 m spacing, planted with a density of 3082 stems/ha; (b) Plot 'Sb', Black Spruce (*Picea mariana*) with 3.6 m spacing, planted with a density of 771 stems/ha; and (c) Plot 'Sb2', Black Spruce (*Picea mariana*) with 1.8 m spacing, planted with a density of 3082 stems/ha. For our study, we only used data acquired for the plots marked with a gold star in Appendix 1. Below, Figure 2.1 shows the site conditions for plots Pr (Figure 2.1(a)), Sb (Figure 2.1(b)), and Sb2 (Figure 2.1(c)).

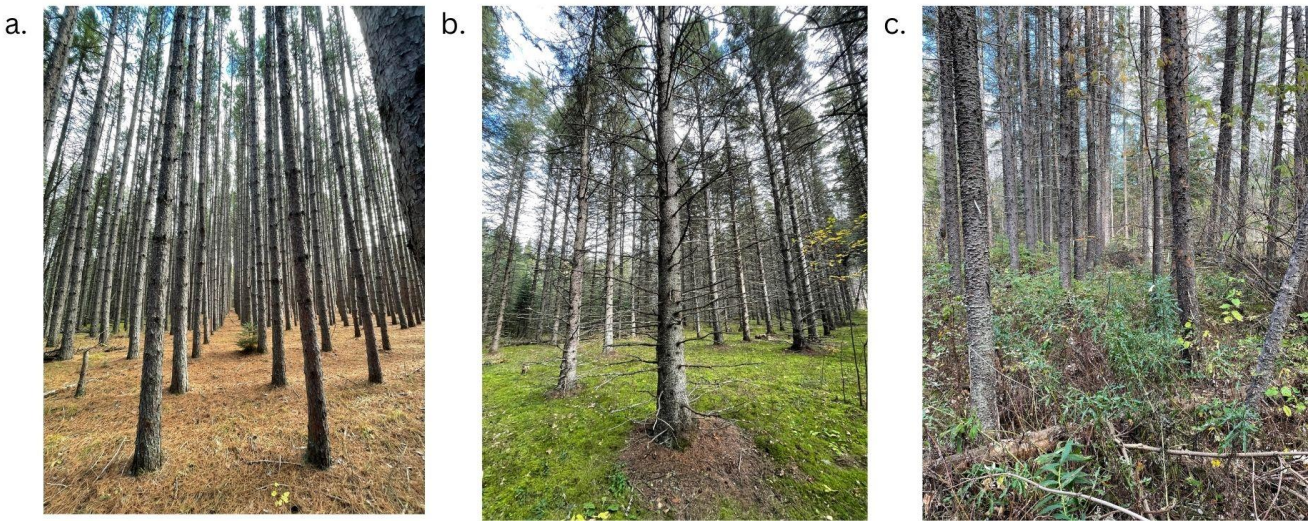


**Figure 2.1.** Images of the stands where plots Pr (a), Sb (b), and Sb2 (c) were performed.

There was no understory or ingrowth in the Pr and Sb sites, while there was some understory and ingrowth in the Sb2 site (Figure 2.1(c)).

### 2.2.2. Data Acquisition

Plot centres were randomly located within each selected stand, and marked using a metre stick with orange flagging tape. These plots were 10 m in diameter, corresponding to an area of 78.54 $m^2$. Each tree in a plot was assigned a number, 'Tree 1' being the tree closest to the plot centre bearing northeast. Tree position within each plot was recorded manually with a compass and measuring tape as the distance (m) and bearing (degrees) from the plot centre to the nearest point on each tree stem. The DBH of each tree in each plot was then measured manually (with a diameter tape) for validation. LiDAR data was acquired for each plot using the iOS application Zappcha with an iPad Pro 12$^{th}$ Generation LiDAR scanner, using three different walking patterns (Circular, Figure-8, Transect) while scanning (Apple 2020; Veesus 2022). The LiDAR device was in continuous motion for the tested scanning patterns while capturing data.

As the circular scanning pattern captured many points, leading to large file sizes, it was necessary to divide each plot into four quadrants (Northeast, Southeast, Southwest, Northwest) and capture individual point clouds for each quadrant. Among the point cloud capture methods available in the Zappcha app, the 'continuous scanning' option was used for this project as this option allowed the greatest maximum scanning range (5 m) (Veesus 2022). The other methods available (burst scan, timed scan) did not capture data continuously, and did so at a maximum scanning range of 2 m.

Since the visited stands were established in 1950, tree mortality has resulted in stand densities differing from the initial stand densities. As a result, the observed stand density (stems/ha) was calculated using the number of trees in each plot.

### 2.2.3. Point Cloud Processing

Raw point clouds acquired at the site were saved to the Zappcha Cloud service and later imported to the CloudCompare software for further processing (Veesus 2022; Girardeau-Montaut 2022).

The point clouds were projected using ArcGIS Pro, and areas of the point cloud that fell outside plot boundaries were removed (ESRI 2023). The Point clouds acquired with the circular scanning pattern for each quadrant of a plot were combined. Outliers were removed from each point cloud in CloudCompare software with the 'Statistical Outlier Removal (SOR)' tool (Girardeau-Montaut 2022). The SOR tool calculates the mean distance from each point in a point cloud to the nearest $k$ neighbours and preserves points within a range of $n$ standard deviations plus the mean neighbour distance for the dataset ($k$=6 and $n$=1) (Girardeau-Montaut 2022). CSF was used to identify the ground elevation of each site, and extract cross-sections of the point cloud centred 1.3 m above the identified ground elevation with thicknesses of both 4 cm and 10 cm (Zhang et al. 2016). These sizes were selected to account for an error of up to 1 cm in estimating the breast height elevation due to the cloth mesh resolution and classification threshold, as well as to evaluate the accuracy of different cross-section sizes.

For the single slice method, point cloud cross-sections were centred 1.3 m above ground. Based on the methods used by Liu et al. (2021), DBH was also estimated using the average diameter of each stem at multiple heights. The cross-sections used for this method were centred at 0.7 m, 1.0 m, 1.3 m, 1.6 m, and 1.9 m above the ground. The cross-sections at 0.7 m and 1.9 m were considered a pair, as were those at 1.0 m and 1.6 m. For both single- and multiple-cross-section methods, cross-sections of 4 cm and 10 cm thickness were extracted, and rasterized with a spatial resolution of 0.05 cm. These rasters showed a circular/elliptic pattern representing individual trees. For further processing, these raster files were converted to point shapefiles.

### 2.2.4. Extracting Cross-Sections

Points representing individual trees in the shapefiles were identified and segmented using density-based clustering (DBSCAN) in ArcGIS Pro, which can detect clusters of points with arbitrary geometries in two or more dimensions (ESRI 2023; Wang et al. 2019). Each unique cluster identified by this tool was segmented into a separate shapefile (ESRI 2023). Figure 2.2 shows a summary of this process for plot 'Sb', showing a point cloud acquired with the circular scanning method and clipped to plot boundaries (Figure 2.2a), the non-ground features point cloud with points in a single 4 cm cross-section at breast height highlighted in black (Figure 2.2b), as well as the DBSCAN output identifying unique clusters of points in each cross-section, with each cluster shown in a unique colour and representing a single tree (Figure 2.2c).

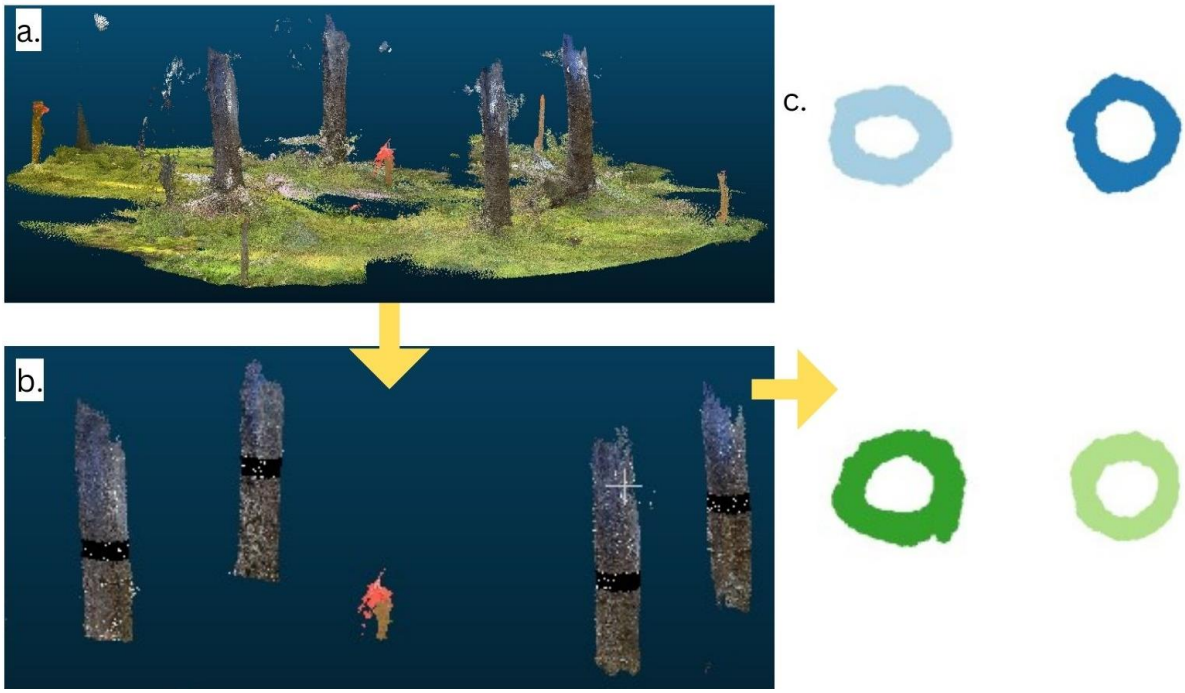


**Figure 2.2.** Processing summary for Plot 'Sb': (a) point cloud acquired with circular scanning pattern; (b) filtered non-ground point cloud with single 4 cm cross-section at breast height highlighted in black; and (c) clusters of points representing individual trees identified by HBDSCAN, with each colour representing a different tree.

In order to pair the shapefiles created for each tree cross-section with the validation dataset for that tree, stem maps were created showing the position of each tree stem within each plot. These stem maps scaled tree stems according to the measured DBH for, as well as numbering each tree to facilitate pairing with the shapefile representing that tree. Figure 2.3 shows the stem map created for Plot 'Pr' in green, as well as a single 4 cm cross-section acquired with the circular scanning pattern for each tree.

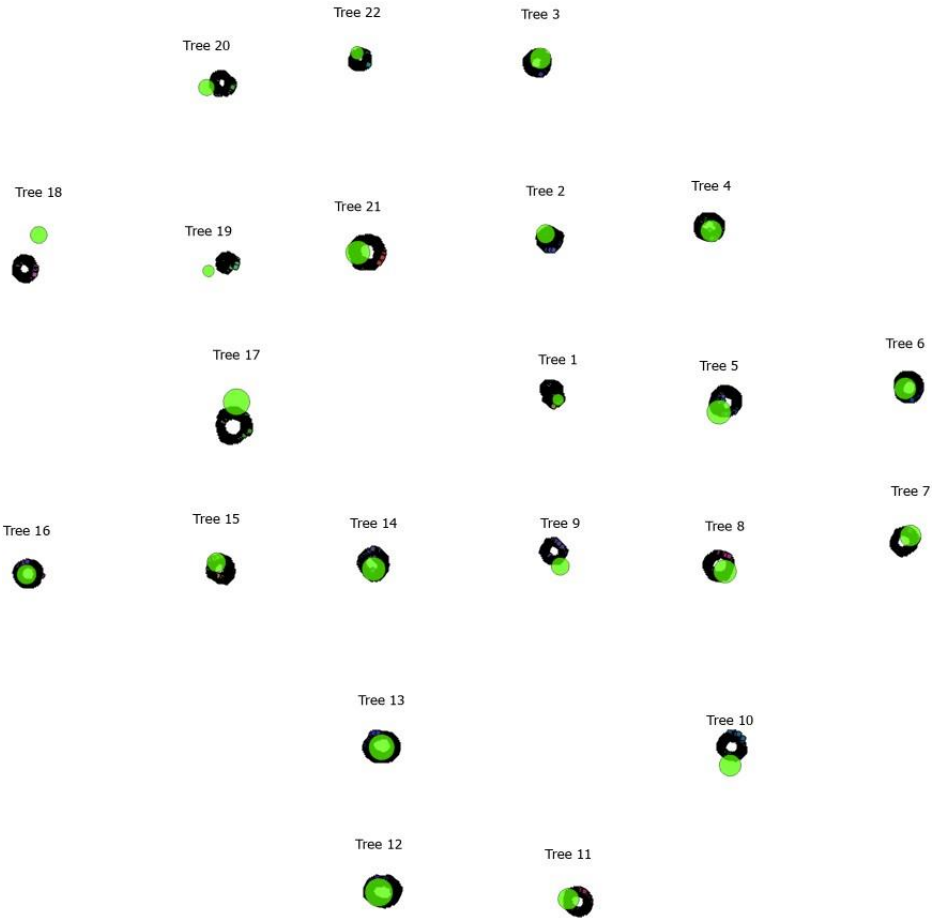


**Figure 2.3.** Stem map for Plot 'Pr' (Green) and the DBSCAN output showing how the validation data was paired to the corresponding tree shapefile.

### 2.2.5. Estimating DBH

X and Y coordinates for each point in the shapefiles were appended to the file attribute tables for the shapefiles representing individual trees. For the multiple slice

methods, if no points for a tree were present at a given height, the shapefile representing cross-section at the paired height was removed to minimize the estimate bias. The attribute table for each tree shapefile was exported to (MathWorks 2022).

Four algebraic curve-fitting formulas were applied to the $X$ and $Y$ coordinates of the points in each tree shapefile to estimate the diameter of the cross-section. The diameters estimated with each of the four fitting functions were averaged for each tree. For the multiple slice methods, DBH was calculated as the average of the diameter estimates for all cross-sections of a given tree. If no points were present for a given tree at a certain height, the DBH estimate from the paired height were discarded to prevent skewing estimates.

### 2.2.6. Accuracy Assessment

The estimated DBH values for each tree were compared with the field-measured DBH using two metrics. Absolute error (Difference between field-measured DBH and estimated DBH in cm) was calculated for each tree. Root Mean Square Error (RMSE) and relative Root Mean Square Error (rRMSE; RMSE as a percentage of the mean DBH value of the individual plot) were calculated for each unique combination of plot, scanning pattern, cross-section count, cross-section size, and curve-fitting formula.

Exploratory data analysis was done for individual tree absolute error values (LiDAR estimated DBH and field measurements) to check whether they were normally distributed. As they were not normally distributed, Kruskal-Wallis tests were performed to test if scanning pattern, cross-section count, cross-section size, or curve-fitting formula had statistically significant impacts on individual tree absolute error. Tests were also performed for each combination of two or more of the above independent variables. This also quantified the significance of each independent variable or pairwise interaction between two or more independent variables. Additionally, a Kruskal-Wallis test was performed to determine the significance of the

relationship between stand density (stems/ha) and estimate accuracy (Individual tree absolute error).

## 2.3. RESULTS

### 2.3.1. Validation Data

Table 2.1 presents the number of trees measured in each plot, as well as the initial and observed site densities and the mean measured DBH for each plot.

**Table 2.1.** Characteristics of each field plot.

| Plot | Number of Trees | Initial Stand Density (stems/ha) | Observed Stand Density (stems/ha) | Mean Measured DBH (cm) |
|---|---|---|---|---|
| Pr | 22 | 3082 | 2801 | 21.71 |
| Sb | 4 | 3082 | 2037 | 25.53 |
| Sb2 | 16 | 771 | 509 | 14.69 |

### 2.3.2. DBH Estimation

Table 2.2 displays the minimum, mean, and maximum estimated DBH values (averaged for each combination of scan pattern, cross-section size, cross-section count, and curve-fitting formula) for each plot, as well as the mean measured DBH. This highlights the range of deviation about the mean measured DBH for each plot.

**Table 2.2.** Mean measured DBH and minimum, mean, and maximum estimated DBH (cm) for each plot with associated estimation methods.

| Plot | Number of Trees | Mean measured DBH (cm) | Estimated DBH (cm) | | |
|---|---|---|---|---|---|
| | | | Minimum | Mean | Maximum |
| Pr | 22 | 21.71 | 15.93 Transect scan, multiple 4cm CS, Taubin's direct ellipse fit | 20.88 | 23.01 Transect scan, single 4cm CS, Pratt's direct circle fit |
| Sb | 4 | 25.53 | 22.55 Figure-8 scan, single 10cm CS, Szpak's ellipse fit | 25.28 | 28.01 Transect scan, multiple 4cm CS, Pratt's direct circle fit |
| Sb2 | 16 | 14.69 | 9.04 Figure-8 scan, single 4cm CS, Taubin's direct ellipse fit | 14.08 | 16.86 Circle scan, multiple 10cm CS, Pratt's direct circle fit |

Table 2.3 presents the distribution of the individual tree absolute error values by scanning pattern, showing the minimum, 1st quartile, median, mean, 3rd quartile, and max absolute errors (cm) achieved by any processing method.

**Table 2.3.** Distribution of absolute error (cm) values by scanning pattern.

| Scanning Pattern | Min. | 1st Qu. | Median | Mean | 3rd Qu. | Max |
|---|---|---|---|---|---|---|
| Circular | 0.00 | 0.53 | 1.05 | 1.51 | 1.80 | 10.26 |
| Figure-8 | 0.16 | 0.90 | 1.86 | 2.84 | 3.63 | 24.32 |
| Transect | 0.00 | 0.79 | 2.01 | 3.16 | 4.33 | 27.52 |

### 2.3.3. Evaluating the Significance of Different Experimental Factors

Table 2.4 presents the results of Kruskal-Wallis tests that were used to determine the level of statistical significance that the tested scanning patterns, cross-section counts,

cross-section sizes, and curve-fitting formulas had on DBH estimate accuracy (individual tree absolute error). Results were reported individually for each independent variable and for interactions between two or more independent variables with a moderate or significant magnitude of effect.

**Table 2.4.** Kruskal-Wallis Test results testing the significance of Scanning Pattern, Cross-Section Size, Cross-Section Count, and Curve-Fitting Formula on individual tree absolute error.

| Factor(s) | Df | Test Statistic | p-Value | Effect Size | Magnitude |
|---|---|---|---|---|---|
| Scanning pattern | 2 | 149.12 | $4.16^{-33}$ | 0.075 | Moderate |
| Cross-Section Size | 1 | 3.97 | 0.05 | 0.002 | Small |
| Cross-Section Count | 1 | 12.89 | $3.31^{-04}$ | 0.006 | Small |
| Fitting Formula | 4 | 29.78 | $5.43^{-06}$ | 0.013 | Small |
| Scan pattern x CS Size | 5 | 162.04 | $3.64^{-33}$ | 0.080 | Moderate |
| Scan pattern x CS Count | 5 | 188.48 | $8.26^{-39}$ | 0.094 | Moderate |
| Scan Pattern x Fitting Formula | 14 | 213.83 | $8.13^{-38}$ | 0.103 | Moderate |
| Scan pattern x CS Size x CS Count | 11 | 204.28 | $9.64^{-38}$ | 0.099 | Moderate |
| Scan pattern x CS Size x Fitting Formula | 29 | 229.01 | $5.69^{-33}$ | 0.104 | Moderate |
| Scan pattern x CS Size x CS Count x Fitting Formula | 59 | 282.97 | $5.40^{-31}$ | 0.118 | Moderate |

*CS= Cross-Section.

The results highlight that the scanning pattern had a moderate effect on individual tree absolute error. Cross-section size, cross-section count, and fitting formula had small effects on the accuracy of the DBH estimates. All two- or three-way interactions involving scan patterns also had moderate magnitudes of effect. As the scanning pattern was the only independent variable to have a moderate effect on

absolute error on its own, a Dunn-Bonferroni test was conducted to determine the significances of differences between scanning methods.

**Table 2.5.** Dunn-Bonferroni test results showing statistical significances of differences between scanning methods.

| Group 1 | Group 2 | Statistic | Adjusted p-Value | Adjusted Significance |
|---|---|---|---|---|
| Circle | Figure-8 | 8.53 | $4.29^{-17}$ | < 0.001 |
| Circle | Transect | 11.30 | $1.09^{-29}$ | < 0.001 |
| Figure-8 | Transect | 0.51 | 0.61 | Not Significant |

As Table 2.5 shows, the circular scanning pattern resulted in estimate accuracies significantly different from those of both the figure-8 and transect scanning patterns, while the figure-8 and transect scanning patterns did not significantly differ in their effects on estimate accuracy.

In addition to the tested independent variables, a Kruskal-Wallis test was also performed to test the significance of observed stand density on estimated DBH accuracy.

**Table 2.6.** Kruskal-Wallis results showing the significance of stand density on individual tree absolute error.

| Factor | Df | Test Statistic | p-Value | Effect Size | Magnitude |
|---|---|---|---|---|---|
| Stand Density | 2 | 26.36 | $1.89^{-06}$ | 0.012 | Small |

Table 2.6 shows that the observed stand density had a small impact on the accuracy of DBH estimates. Table 2.7 compares the individual tree absolute error values (cm and %), averaged across all plots and curve-fitting formulas for each combination of scanning pattern, cross-section count, and cross-section size. The circle scanning pattern provided the most accurate DBH estimates, and the transect pattern provided the least accurate DBH estimates. When using the circle scanning pattern, the single 4

cm cross-section led to the most accurate estimates, while the multiple 10 cm cross-sections led to the most accurate estimates in both figure-8 and transect patterns.

**Table 2.7.** Mean absolute error at the individual tree level as a function of the scanning pattern, cross-section count, and cross-section size. Bold figures represent the optimal combination for each scanning pattern.

| Scanning pattern | Cross-Section Count | Cross-Section Size (cm) | Mean Absolute Error (cm) | Relative Error (%) |
|---|---|---|---|---|
| **Circle** | **Single** | **4** | **0.99** | **5.11** |
| | Single | 10 | 1.35 | 6.95 |
| | Multiple | 4 | 1.90 | 9.80 |
| | Multiple | 10 | 1.79 | 9.22 |
| Figure-8 | Single | 4 | 3.51 | 21.00 |
| | Single | 10 | 2.77 | 16.53 |
| | Multiple | 4 | 2.72 | 16.24 |
| | **Multiple** | **10** | **2.38** | **13.92** |
| Transect | Single | 4 | 3.57 | 21.34 |
| | Single | 10 | 2.60 | 21.34 |
| | Multiple | 4 | 3.32 | 17.08 |
| | **Multiple** | **10** | **3.16** | **16.25** |

Table 2.8 presents the mean absolute error (cm and %) for each combination of scanning pattern and curve-fitting formula, averaged across all plots, cross-section counts, and cross-section sizes.

**Table 2.8.** rRMSE (%) for each combination of scanning pattern and curve-fitting formula. Bold values indicate optimal rRMSE (%) for each scanning pattern.

| Scanning pattern | Curve-Fitting Formula | Mean Absolute Error (cm) | Relative Error (%) |
|---|---|---|---|
| Circular | Pratt's Direct-Least Squares Circle | 1.56 | 8.03 |
| | **Taubin's Direct-Least Squares Circle** | **1.33** | **6.85** |
| | Taubin's Direct-Least Squares Ellipse | 1.48 | 7.62 |
| | Szpak's Ellipse Fit with Sampson Method | 1.81 | 9.35 |
| | Combined Formula | 1.36 | 6.99 |
| Figure-8 | **Pratt's Direct-Least Squares Circle** | **2.15** | **12.81** |
| | Taubin's Direct-Least Squares Circle | 2.37 | 14.07 |
| | Taubin's Direct-Least Squares Ellipse | 3.43 | 20.40 |
| | Szpak's Ellipse Fit with Sampson Method | 3.82 | 22.74 |
| | Combined Formula | 2.40 | 14.30 |
| Transect | Pratt's Direct-Least Squares Circle | 2.60 | 15.48 |
| | Taubin's Direct-Least Squares Circle | 2.58 | 15.48 |
| | Taubin's Direct-Least Squares Ellipse | 4.32 | 22.10 |
| | Szpak's Ellipse Fit with Sampson Method | 3.76 | 19.27 |
| | **Combined Formula** | **2.54** | **12.98** |

As stands in a natural forest will vary in density (stems/ha), a weighted average of RMSE was calculated for the three plots as follows:

Average RMSE = [(22 trees * Plot 'Pr' mean RMSE) + (4 trees * Plot 'Sb' mean RMSE) + (16 trees * Plot 'Sb2' mean RMSE)] / 42 trees.

Table 2.9 presents the average and optimal RMSE (in cm) and the rRMSE for each scanning pattern, averaged for all plots, cross-section counts, cross-section sizes, and curve-fitting formulas. It shows the circular scanning pattern, using a single 4 cm

cross-section and a combination of all four curve-fitting formulas as the combination of data acquisition and processing methods provides the most accurate estimates of DBH. The use of a single 4 cm cross-section with Pratt's direct least-squares circle fit led to the most accurate estimates of DBH with the figure-8 scanning pattern. Processing the data with multiple 4cm cross-sections and a combination of all tested curve-fitting formulas provided the most accurate estimates of DBH for the transect scanning pattern.

**Table 2.9.** Average and optimal RMSE (cm) and rRMSE as a function of the scanning pattern.

| Scanning pattern | RMSE (cm) | | rRMSE (%) | | Estimation method producing optimal RMSE |
|---|---|---|---|---|---|
| | Mean | Optimal | Mean | Optimal | |
| Circular | 2.01 | 1.13 | 11.24 | 6.17 | Average of all formulas & single 4cm CS. |
| Figure-8 | 3.85 | 1.68 | 24.52 | 10.17 | Pratt's least-squares circle fit & single 4cm CS. |
| Transect | 4.29 | 3.12 | 23.86 | 17.05 | Average of all formulas & multiple 4cm CS. |

In order to model the relationship between actual and estimated DBH, these values for all trees were plotted with a line showing a 1:1 relationship (Figure 2.4). Figure 2.4 shows that the circular scanning pattern produced estimates consistently near the line modelling the 1:1 relationship, with outliers coming from the figure-8 or transect scanning patterns using single cross-sections.

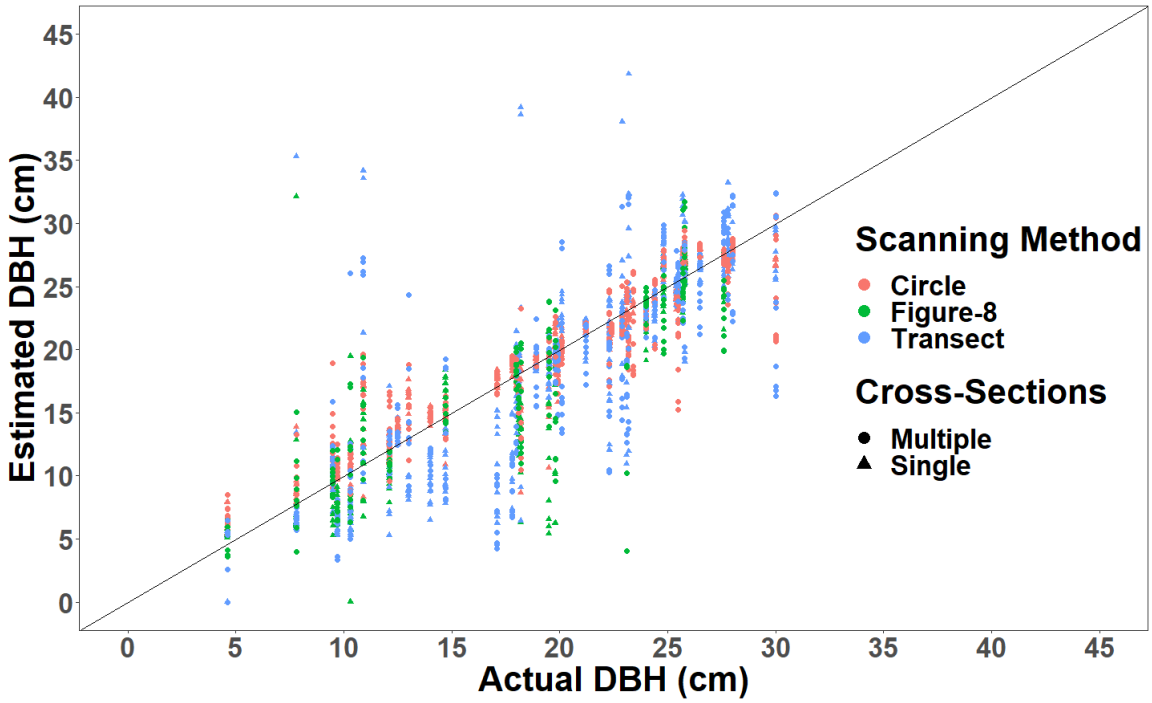


**Figure 2.4.** Data acquisition patterns and walking paths (a) circular; (b) figure-8; and (c) transect scanning patterns. The walking path for each scanning method is displayed in red and the scanning direction is indicated with a blue arrow.

Based on Figure 2.4, the circular scanning pattern produced most accurate estimates of DBH across the range of actual DBH values present in the data. Figure-8 and transect scanning patterns resulted in the majority of the outliers, especially when only one stem cross-section was used.

### 2.3.4. Scanning Errors with iPad Pro LiDAR

Due to the nature of the walking path for the transect scanning pattern (Figure 2.1c), each tree was scanned on two separate passes around the plot, potentially causing accumulated positioning errors. The literature shows there are known Inertial Measurement Unit (IMU) drift, rotational, and GPS positional errors with the iPad Pro LiDAR scanner that may cause issues in acquired point clouds (Wang et al. 2021; Corradetti et al. 2022; Tavani et al. 2019). An example of this is highlighted in Figure 2.5, which shows the top view of the 4 cm single cross-sections of the same tree in the Sb plot for different scanning patterns: circular (2.5a), figure-8(2.5b), and transect (2.5c).

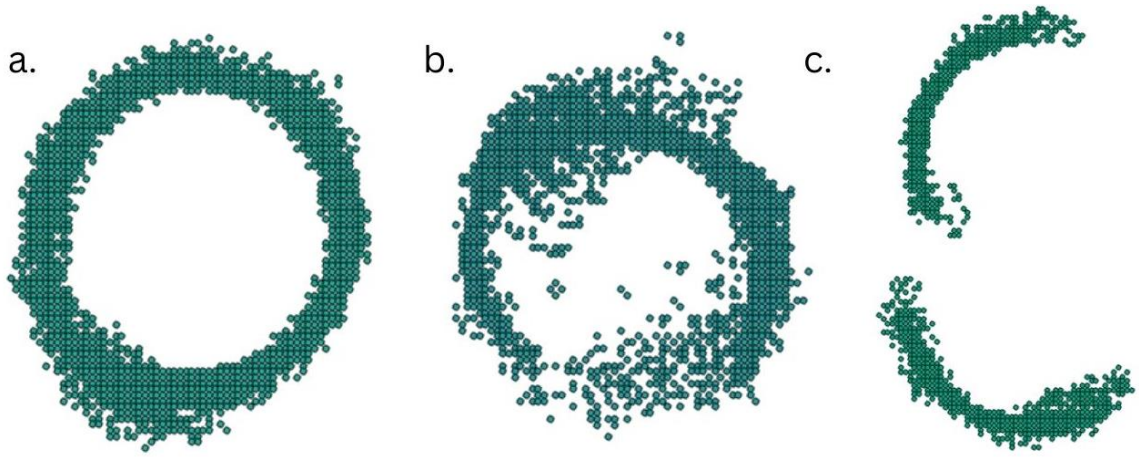


**Figure 2.5.** Data acquisition patterns and walking paths (a) circular; (b) figure-8; and (c) transect scanning patterns. The walking path for each scanning method is displayed in red and the scanning direction is indicated with a blue arrow.

As seen in Figure 2.5a, the circular scanning pattern resulted in a cross-section showing the entire circumference of the tree with few outliers. The figure-8 scanning pattern (Figure 2.5b) resulted in a cross-section representing most of the stem circumference, with some outliers. The transect scanning pattern (Figure 2.5c) showed a cross-section consisting of two separate sections, each of which represented only half of the stem's circumference, indicating some locational errors.

Figure 2.6 shows cross-sections of Tree 9 in Plot 'Pr', extracted from point clouds acquired with the circular scanning pattern (a) and transect scanning pattern (b). For both cross-sections, the tree centroid point and results of Pratt's circle fit (Red line) and Szpak's ellipse fit (Blue line) are shown.

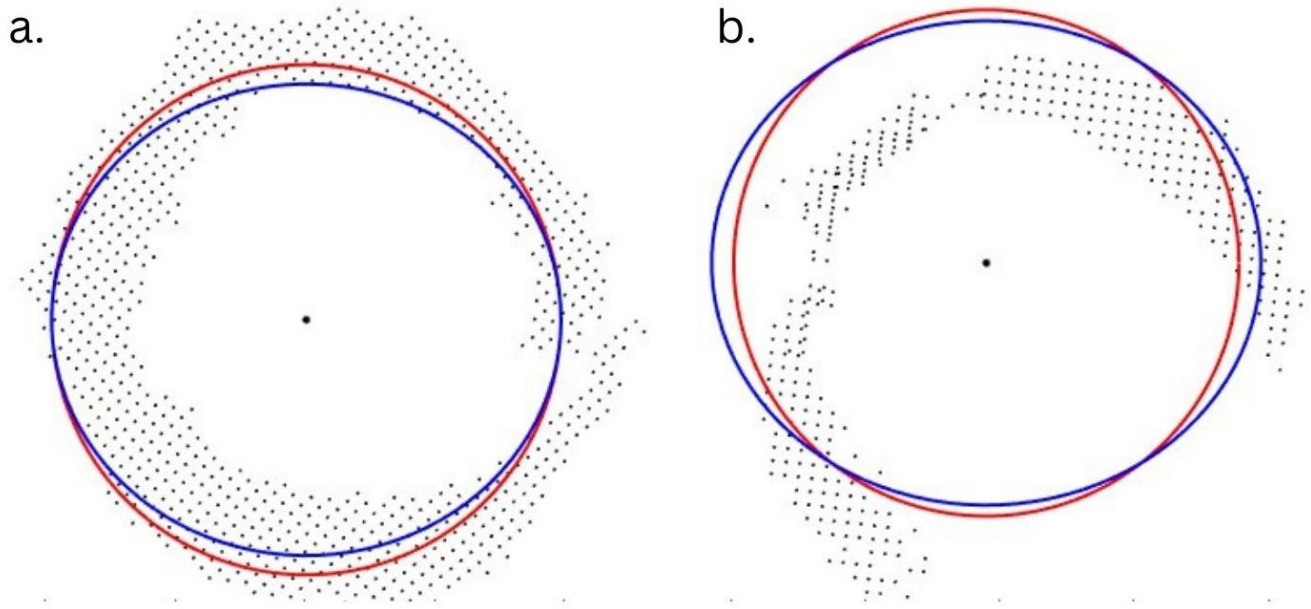


**Figure 2.6.** Plotted stem cross-sections and centroid points (black circle) extracted from a circular scanning pattern point cloud (a) and a transect scanning pattern point cloud (b), with plotted results for Pratt's circle fit (red) and Szpak's ellipse fit (blue).

As Figure 2.6 shows, the circular scanning pattern provided a feasible stem centroid location, while the transect pattern did not. Additionally, the fitted curves aligned with the stem cross-section extracted from the circular scanning pattern but not the transect cross-section.

## 2.4. DISCUSSION

### 2.4.1. DBH Estimation Accuracy

The circular scanning pattern produced the lowest optimal and average absolute error (Table 2.9), while also resulting in the lowest overall values for individual tree absolute error (Table 2.3). Due to the irregular and inconsistent shapes of tree stems, the greater the distribution of stem points about the circumference of each tree in the point cloud, the more accurate the estimates of DBH were (Hunčaga et al. 2020). When a combination of circle- and ellipse-fitting formulas were applied to a single 4cm cross-section, an RMSE of 1.13 cm (rRMSE of 6.17%) was achieved. This method produced a

lower RMSE value than those reported in many other studies using the iPad Pro LiDAR scanner for DBH estimation. For example, Gollob et al. (2020) report RMSE (rRMSE) values between 3.13 cm (10.50%; ellipse fit) and 6.29 cm (21.23%; cylinder fit) using the Polycam and SiteScape iOS Applications for an iPad Pro 12th Generation. They applied ellipse- and cylinder-fitting formulas to 15 cm cross-sections and were able to acquire point clouds with a scanning pattern similar to the circular scanning pattern (Figure 2.2a) used in this study. Wang et al. (2021) reported RMSE (rRMSE) values between 2.78 cm (7.27%) and 5.18 cm (13.03%) in an urban forest using the 3D Scanner iOS application for the iPad Pro to acquire data, using the optimal circle fit formula in DendroCloud to extract DBH. Chiappini et al. (2022) achieved RMSE (rRMSE) values of 4.1 cm (16.3%) with the 3D Forest iOS application, 6.8 cm (27.0%) with the VoxR package in R, and 2.7 cm (10.0%) using a convex hull fit with the "TreeLS-lidr-rLiDAR" package in R. Tatsumi et al. (2021) achieved RMSE (rRMSE) values of 2.3 cm (10.3%) using the ForestScanner iOS Application on an iPhone 13 Pro and 2.3 cm (10.5%) using the same application with an iPad Pro 2021. A previous study at the 25th Sideroad Site obtained RMSE (rRMSE) values between 2.82 cm (12.82%) and 5.9 cm (26.82%) by manually fitting curves to point clouds acquired with the iPad Pro 12th Generation (Wang et al. 2022).

Our method did generate results comparable to those achieved with higher-quality terrestrial LiDAR scanners. For example, Liu et al. (2021) reported RMSE (rRMSE) values between 1.97 cm (6.35%; urban forest) and 3.17 cm (13.21%; natural forest) using a Velodyne VLP-16 LiDAR sensor, with a range of up 100 m and an accuracy of ±3 cm. In their study, they used a RANSAC circle-fitting formula applied to 7 stem cross-sections. In another study, Gollob et al. (2020) report RMSE (rRMSE) values of 1.59 cm (6.29%; circle fit) to 2.07 cm (8.29%; cylinder fit) using a GeoSLAM ZEB HORIZON scanner with a maximum range of 100 m and an accuracy of ±3 cm. Our results support previous findings that the circular scanning pattern results in the most

accurate DBH estimates (i.e., with the lowest rRMSE values). The circular scanning pattern also resulted in more consistent DBH estimation accuracies, with a lower maximum error than the other scanning patterns (Table 2.3).

For the circular scanning pattern, both tested single cross-section methods were more accurate than the multiple cross-section methods for all tested plots. For the figure-8 and transect scanning patterns, the multiple cross-section methods did, however, lead to improved DBH estimate accuracy. This is consistent with the findings of Liu et al. (2021), who observed improved DBH estimate accuracy using multiple stem-cross sections in comparison to single cross-sections.

Our study allows to conclude that the circular scanning pattern, using a combination of different curve-fitting formulas applied to a single 4 cm cross-section of the stem represents the optimal combination for extracting DBH using iPad Pro LiDAR sensor.

### 2.4.2. Scanning Errors with iPad Pro LiDAR

The irregular geometry of tree stems, the presence of noise (i.e., points in a point cloud that did not represent features in the correct location), IMU drift, and rotational errors within the acquired point clouds are possible explanations for the low accuracy for the figure-8 and transect scanning patterns. Szpak et al. (2015) noted that at least 400 points representing 50% or more of the curve circumference were necessary for their ellipse fit to produce reliably accurate results. Many cross-sections extracted from point clouds acquired with the transect scanning pattern tend to have fewer than 200 points, with less than 50% of the stem circumference being represented. The figure-8 scanning pattern offered an improvement over the transect pattern with respect to both the number of points associated with each tree stem cross-section and in the proportion of tree circumference represented. However, both patterns resulted in a greater number of

inaccurate placement of points in the acquired datasets (Figures 2.6b and 2.6c) compared to those of the circular scanning pattern (Figure 2.6a).

Positional errors, caused by factors such as Inertial Measurement Units (IMUs) or the device GPS, may have contributed to inaccurate location of acquired points with the iPad Pro LiDAR scanner (Luetzenburg et al. 2021). Previous studies have found iPad and iPhone LiDAR scans result in "crude" 3-dimensional models with low surface fidelity due to accumulated IMU errors (Corradetti et al. 2022; Tavani et al. 2019). Over the course of a scan, previous studies have found the factor by which points are incorrectly located within a cloud to reach up to 2 m (Castel and D'Hoedt 2022). While Tavani et al. (2019) suggest the use of multiple ground control points and post-processing to correctly align and scale point clouds, this was not performed in this study, potentially contributing to the observed errors.

The four curve-fitting formulas used in this determined the centroid coordinates (a, b) of each fitted curve as the average X and Y values in each dataset (Pratt 1987; Taubin 1991; Szpak et al. 2015). As a result, increasing the proportion of noise points within each tree cross-section was found to correspond with an increase in the misplacement of the stem centroid.

### 2.4.3. Impact of Stand Density

In this study, a Kruskal-Wallis test showed that site density had a small impact (p-value =1.89 x 10-6, effect size = 0.012) on estimate accuracy. This was a greater significance than the cross-section sizes and counts, but less significant than the scanning pattern or fitting formula used. There was additionally no observed pattern in the interaction between stand density and estimate accuracy. In a study regarding initial tree spacing and DBH at the study site, a highly significant difference ($p<0.01$) in DBH values between initial spacing distances was observed (McClain et al. 1994). Based on this result, a regression was performed, testing the relationship between individual

tree size and estimate accuracy. A strong, positive correlation was observed between estimate accuracy and increases in measured DBH (cm, R=0.98), which is consistent with previous findings (Wang et al. 2022; Liu et al. 2021; Chen et al. 2022). The differences between correlation versus causation in the relationships between stand density, measured stem size, and estimate accuracy were not explored.

## 2.5. CONCLUSION

Our study suggests that the circular scanning pattern with a single 4cm cross-section and a combination of circle- and ellipse- fitting formulas produced the most accurate DBH values over a range of observed stand densities. RMSE values as low as 1.13 cm (6.17% of mean plot DBH) were achieved with this method. DBH estimate accuracy was found to have no correlation with site density (stems/ha; $R^2$=0.18) and a strong positive correlation with increases in stem size (cm; $R^2$=0.96).

Boreal forest landscapes continue to be dominated by natural (wildfire origin) stands, as opposed to uniformly-spaced, intensively managed plantations. Therefore, our future research to expand on the findings of this study will extend to stands representing a range of natural boreal forest conditions to evaluate the feasibility, in terms of accuracy and efficiency, of DBH estimation. This research will include an examination of how different stand conditions such as the presence of understory vegetation (i.e., medium to tall shrubs), stand age (i.e., differences in horizontal and vertical complexities), and stand species composition (e.g., broadleaf- or conifer-dominant and mixed wood) impact the accuracy of DBH estimates. Further, a workflow for operationalizing the use of iPad Pro LiDAR for DBH estimation in forest inventories should also be developed.

# CHAPTER 3: TREE DIAMETER AT BREAST HEIGHT (DBH) ESTIMATION USING AN IPAD PRO LIDAR SCANNER: A CASE STUDY IN BOREAL FORESTS, ONTARIO, CANADA[2]

## 3.1. STUDY INTRODUCTION

As identified in the Introduction (Chapter 1), no studies have yet used the iPad Pro LiDAR scanner to estimate DBH for trees in natural boreal forests in Canada. Therefore, this study examined a range of natural boreal forest sites to investigate the feasibility of using the optimal methodology identified in Chapter 2 to estimate DBH in natural forest conditions. Specific objectives of this study were to: (1) determine if site-level attributes (Age Class, Species Class, Tree Density, Understory Density) or tree-level attributes (Tree Species, DBH sizes) have statistically significant impacts on DBH estimate accuracy; and, (2) identify site- or tree-level attributes that facilitate or inhibit accurate estimates of DBH from LiDAR point cloud data. It is hypothesised that DBH estimate accuracy will be reduced in stands with significant leafy tissue at or around breast height, either sites with high understory densities or sites with high site densities (trees per ha). It is also hypothesised that DBH estimate accuracy at the individual tree level will increase as measured DBH increases , as DBH estimate accuracy was found to increase as measured DBH increases (Chapter 2).

## 3.2. MATERIALS AND METHODS

### 3.2.1. Study Area

LiDAR and model validation data was collected in 15 natural, wildfire-origin stands that represented five age classes (20-40 years, 41-60 years, 61-80 years, 81-100 years, and 101+ years) and three species groups (Broadleaf-dominated sites (BRD): 68-

[2] This chapter was published as Guenther, M.; Heenkenda, M.K.; Morris, D.; Leblon, B. Tree Diameter at Breast Height (DBH) Estimation Using an iPad Pro LiDAR Scanner: A Case Study in Boreal Forests, Ontario, Canada. Forests 2024, 15, 214, doi:10.3390/f15010214.

100% broadleaf, Coniferous sites (CON): 68-100% conifer, and mixed sites (MX): 33-67% conifer). The study sites were located in one of three Forest Management Units (FMUs) that adjoined each other: the Black Spruce, Dog River-Matawin, and English River FMUs. The sites sampled represented a selected sub-sample of the Ontario Ministry of Natural Resources and Forestry (OMNRF) Vegetation Sampling Network (VSN) plots. VSN plots are circular (400 m2), with a radius of 11.28 m from a fixed plot center to the plot boundary. All VSN plot centers are marked on the ground with a metal rod to ensure each field crew visiting the site uses the same plot center. Below, Figure 3.1 shows the location of the sites selected for this study within northwestern Ontario, as well as their location within Ontario.

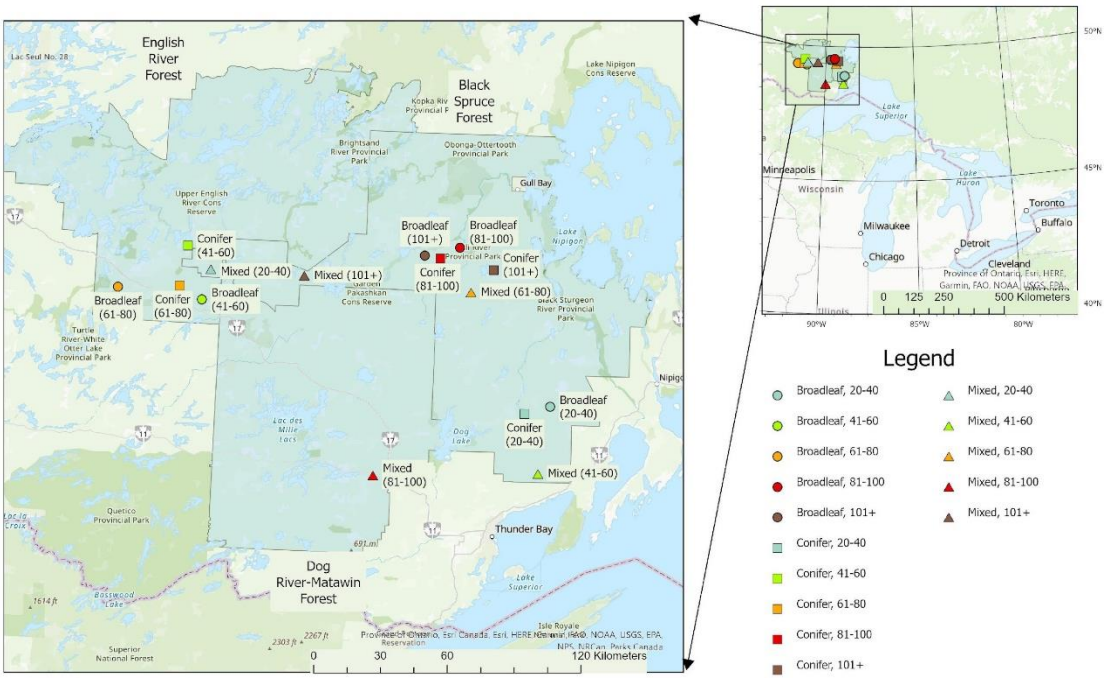


**Figure 3.1.** Map showing location of field sites within northwestern Ontario.

### 3.2.2. Data Acquisition

#### *3.2.2.1. Validation Data*

Validation data was collected by two field crews working independently of one another. Field crews visited each site within three months of one another to ensure site

conditions did not change between visits. The first field crew established the VSN plot (e.g., located the plot centers using preassigned GPS coordinates, flagged the plot boundary), then numbered each tree within the plot boundary with a DBH greater than or equal to 7 cm in the 11.28 m radius VSN plot, and recorded species, status (live versus dead), DBH (recorded to the nearest 0.1 cm using a diameter tape) and height. The field crew also measured 1.3 m above the point of germination for each tree and painted a line at this height, to ensure subsequent measurements of DBH were recorded at the same height.

The second field crew recorded the species, status, and DBH of all trees larger than 7 cm within a smaller subplot (5 m radius) of the VSN plot center. The DBH was recorded to the nearest 0.1 cm using a diameter tape. An average of the two DBH values collected by each of the field crews was used as the validation DBH value for each sampled tree. Distance from plot center was recorded to the nearest point on each tree stem at breast height using a clinometer. The distance (m) and azimuth (Degrees) from the plot center to the nearest point on each tree stem to facilitate correlating validation data with trees in the extracted site cross-sections. Azimuth was recorded to the nearest degree using a compass. For each field site, understory was classified into one of five categories of understory density (Minimal: 0-20% of tree stems between 0 and 2.5 m are obscured; Low: 21-40% obscured; Moderate: 41-60% obscured, Dense: 61-80% obscured, or Very Dense: 81-100% obscured) based on the amount of leafy vegetation present between 0.5 m and 2.5 m above the ground when the point clouds were acquired.

**Table 3.1.** Field Site Overview.

| Site | Age | Measured Trees * | Density (Stems ha-1) ** | Species Composition *** | Average DBH (cm) | Understory Class |
|---|---|---|---|---|---|---|
| BRD 20-40 | 35 | 19 | 2419 | Pt74 Sb26 | 13.1 | Low |
| BRD 41-60 | 45 | 7 | 1019 | Pt80 Pj10 Bw10 | 20.9 | Dense |
| BRD 61-80 | 74 | 9 | 1273 | By50 Mr50 | 16.0 | Moderate |
| BRD 81-100 | 91 | 8 | 1146 | Pt100 | 29.7 | Moderate |
| BRD 101+ | 114 | 3 | 764 | Pt100 | 21.5 | Very Dense |
| CON 20-40 | 27 | 23 | 2928 | Sb91 Pj9 | 10.4 | Low |
| CON 41-60 | 54 | 12 | 1528 | Bf83 Pt17 | 19.5 | Very Dense |
| CON 61-80 | 74 | 2 | 382 | Pj100 | 30.6 | Low |
| CON 81-100 | 91 | 15 | 1909 | Pj100 | 21.9 | Minimal |
| CON 101+ | 105 | 7 | 1146 | Cw78 Bf11 Bw11 | 23.8 | Minimal |
| MX 20-40 | 25 | 8 | 1401 | Pt64 Pj18 Sb16 | 17.4 | Minimal |
| MX 41-60 | 50 | 8 | 1146 | Bf44 Bw22 Sb22 Ag12 | 14.9 | Moderate |
| MX 61-80 | 70 | 2 | 254 | Sw50 Bw50 | 28.4 | Very Dense |
| MX 81-100 | 84 | 6 | 764 | Pt50 Bf30 Sw20 | 28.4 | Dense |
| MX 101+ | 109 | 4 | 764 | Pj66 Pt34 | 25.4 | Minimal |

* Number of measured trees includes only living trees (DBH ≥ 7.0 cm) within the 5 m sub-plot.
** Density calculated using number of living and dead trees (DBH ≥ 7.0 cm) within the 5 m sub-plot.
*** Species composition is represented by two-letter species codes: Pt, trembling aspen (Populus tremuloides); Sb, black spruce (Picea mariana); Pj, jack pine (Pinus banksiana); Bw, white birch (Betula papyrifera); By, yellow birch (Betula alleghaniensis); Mr, red maple (Acer rubrum); Bf, balsam fir (Abies balsamea), Cw, eastern white cedar (Thuja occidentalis); Ag, green ash (Fraxinus pennsylvanica); Sw, white spruce (Picea glauca).

#### *3.3.2.2. LiDAR Data*

To prepare sites for LiDAR acquisition, the metal rod at the plot center was flagged with both pink and yellow flagging tape. The 5 m radius from plot center to the LiDAR subplot boundary in each of the four cardinal directions was measured using a 30m measuring tape. Tripods were placed at the plot boundary in each of the four

cardinal directions to simplify the process of point cloud registration and point matching. The base of all measured, living trees located in each plot were marked with pink flagging tape to facilitate identification of 'in' trees while acquiring LiDAR data. Point clouds were acquired using the Zappcha application and an Apple iPad Pro 12th Generation . The circular scanning method that was found to provide the most accurate estimates of DBH was used for point cloud acquisition (Guenther et al. 2024). Below, Figure 3.2 shows the raw point cloud for site BRD 61-80.

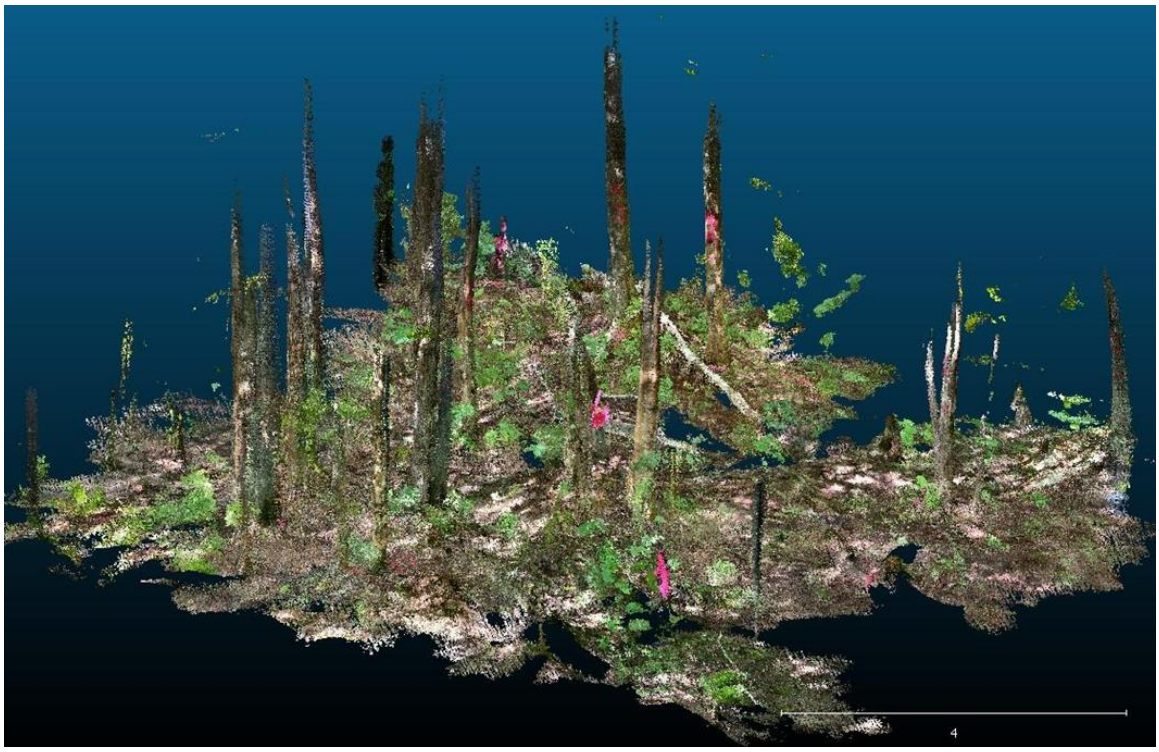

**Figure 3.2.** Raw, unprocessed point cloud for site BRD 61-80.

### 3.2.3. Point Cloud Processing

Point clouds were imported to CloudCompare software from Zappcha app via the Veesus Cloud Plugin for further processing (Veesus 2023; Girardeau-Montaut 2023). The point clouds were projected and clipped to plot boundaries using ArcGIS Pro (ESRI 2023). Using the CloudCompare software, point clouds were co-registered for the quadrants in each plot, then cleaned using the 'Statistical Outlier Removal (SOR)' tool

(Girardeau-Montaut 2023). Figure 3.3 shows the clipped and projected point cloud for site BRD 61-80 after the use of the SOR tool.

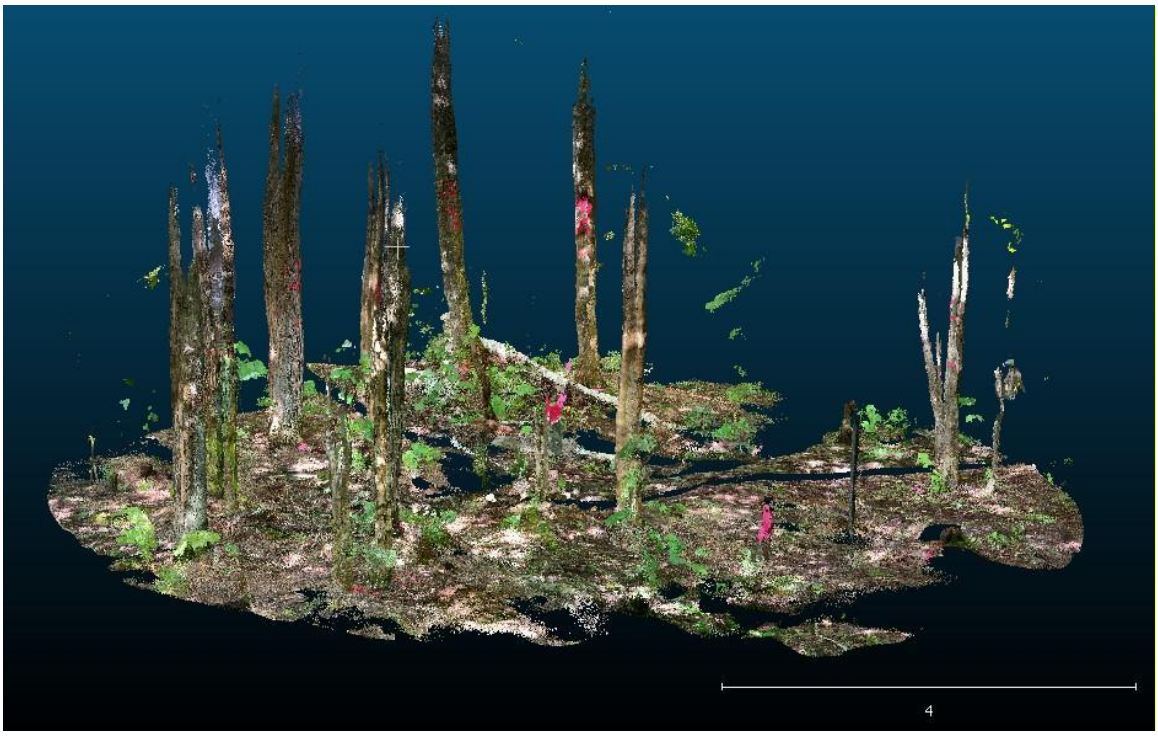


**Figure 3.3.** The projected and clipped point cloud for site BRD 61-80 after the use of the SOR tool.

The Cloth Simulation Filtering (CSF) method developed by Zhang et al. (2016) was used to identify points related to the ground in each filtered point cloud and interpolate the ground surface for areas without data. Using the elevation value for the interpolated ground surface, the elevation value representing breast height (1.3 m above ground) for each point cloud was calculated. A single 4 cm tall cross-section centered at breast height was extracted from each non-ground point cloud. Points representing individual features in plot cross-sections were identified and segmented using the density-based clustering algorithm (DBSCAN) in ArcGIS Pro (ESRI 2023). By cross-referencing the identified clusters with stem maps for each plot, the cluster representing each measured tree was identified. Clusters representing more than one tree were manually split into separate shapefiles. Manual cleaning of the clusters representing

measured trees was performed. The X and Y coordinates of each point in the trimmed cluster shapefiles were appended to the attribute tables.

All tree attributes were imported to R, using the 'conicfit' package for curve fitting (Bivand et al. 2023). An iterative geometric ellipse fit was applied to the points in each stem cross-section (Chernov and Gama 2015). The iterative ellipse fitting formula used the results of Taubin's Direct-Least Squares Ellipse fitting formula as the initial estimated ellipse parameters for each tree. The iterative ellipse-fitting formula then used the Levenberg-Marquardt method with a maximum of 200 iterations to reduce the error metric of the fitted ellipses (Chernov and Gama 2015; Taubin 1991). Using the geometric parameters for each fitted ellipse, the average diameter of each ellipse was calculated as the estimated DBH (cm).

### 3.2.4. Statistical Methods

The average of the DBH values (cm) recorded by the two field crews for each tree were used as the validation DBH values. The difference (cm), absolute error, and relative absolute error between the estimated DBH and the validation DBH were calculated for each tree. The acceptable accuracy level of OMNRF's DBH estimation in forest inventories is 1cm compared to the actual measurements (OMNRF 2021). Hence, this study adapted the same accuracy level.

The absolute error (cm) and relative absolute error (%) of each individual tree were used as measures of accuracy for statistical analyses. Box plots were created for the overall dataset to identify skew and distribution of the results. Kruskal-Wallis tests were used to determine if any of the tested independent variables at the site level (Site type, species class, stand age, stand density, understory class) or individual tree level (tree species, measured DBH size) had statistically significant impacts on the accuracy of estimated DBH values (relative error). For variables with significant impacts on

estimate accuracy, a Dunn-Bonferroni post-hoc test was used to determine how different values of that variable impacted estimate accuracy.

## 3.3. RESULTS

### 3.3.1. Validation Data

The 15 sites varied considerably for live tree density (254 - 2928 stems ha-1), ranged in age from 25-114 years, and had a range of understory densities (Table 3.1). None of the 15 study sites had all estimated DBH values within 1 cm of the measured DBH, ranging from as high as 83.3% (Site MX 81-100) to as low as 0% (Site MX 61-80). The least accurate DBH estimate was a White Spruce (*Picea glauca*) in plot CON 20-40, with an actual DBH of 12.2cm and an estimated DBH of 7.1cm.

**Table 3.2.** Comparison between the mean measured and estimated DBH values (cm) and associated MAE (cm and %) for the 15 visited sites.

| Site Name | Mean Measured DBH (cm) | Mean Estimated DBH (cm) | MAE (cm) | MAE (%) |
|---|---|---|---|---|
| BRD 20-40 | 13.1 | 12.7 | 1.1 | 8.4 |
| BRD 41-60 | 20.9 | 20.9 | 1.3 | 6.2 |
| BRD 61-80 | 16.0 | 15.3 | 1.6 | 10.0 |
| BRD 81-100 | 29.7 | 29.8 | 0.6 | 2.0 |
| BRD 101+ | 18.7 | 17.7 | 1.9 | 10.2 |
| CON 20-40 | 10.4 | 9.4 | 1.0 | 9.6 |
| CON 41-60 | 14.8 | 14.6 | 2.0 | 13.5 |
| CON 61-80 | 30.6 | 31.3 | 0.7 | 2.3 |
| CON 81-100 | 21.9 | 21.9 | 0.9 | 4.1 |
| CON 101+ | 23.8 | 24.8 | 1.1 | 4.6 |
| MX 20-40 | 17.4 | 17.3 | 0.6 | 3.4 |
| MX 41-60 | 14.9 | 13.9 | 1.2 | 8.1 |
| MX 61-80 | 28.4 | 26.9 | 1.5 | 5.3 |
| MX 81-100 | 26.2 | 26.1 | 0.5 | 1.9 |
| MX 101+ | 25.4 | 25.6 | 1.3 | 5.1 |

### 3.3.2. Impact of Site- and Tree-Level Factors on Estimation Accuracy

Overall, an RMSE of 1.5 cm (8.6%), and an MAE of 1.1 cm (6.4%) were achieved in this study. The distribution of the individual tree absolute error values was not normally distributed, and the results skewed towards zero (Figure 3.4).

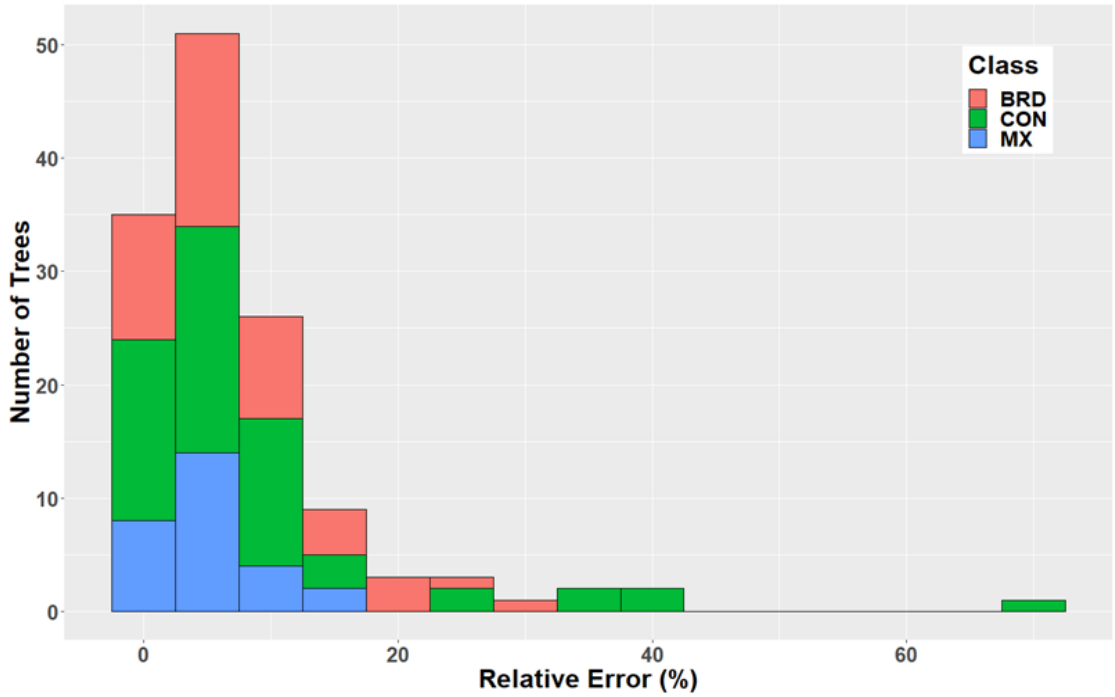


**Figure 3.4.** Histogram showing distribution of the number of trees as a function of the relative error values.

The 81-100 age class produced the most accurate estimates of DBH, with an MAE of 0.72 cm (3.01%) (Table 3.3). In terms of stand density effects, the lowest density class (250-500 stems ha-1) produced the most accurate estimates of DBH in terms of relative MAE, with an MAE of 1.13 (3.92%), although this density class only had 4 measured trees. For density classes with 10 or more measured trees, the most accurate estimates of DBH (cm) were achieved in the 501-1000 stems ha-1 density class, which had an MAE of 1.03 cm (4.59%; Table 3.3). The sites with minimal understory produced the most accurate estimates of DBH, with an MAE of 0.91 cm (4.06%) (Table 3.3). Generally, the MAE were comparable across the understory classes 1 (minimal) to 4 (dense), but

increased substantially in the very dense class (MAE: 19.4 cm and relative MAE of 17.6%). The 25.1-30 cm DBH class produced the lowest MAE (0.82 cm; 3.02%), while the 30.1-35 cm DBH class produced the lowest relative MAE (0.94 cm; 2.97%) (Table 3.3).

**Table 3.3.** Comparison between the mean measured and estimated DBH values (cm) and associated MAE (cm and %) for the 15 visited sites.

| Factor | Factor Level | Number of Trees | Mean Absolute Error (cm) | Relative Mean Absolute Error (%) |
|---|---|---|---|---|
| Species Class | Broadleaf | 46 | 1.19 | 7.30 |
| | Conifer | 59 | 1.16 | 9.45 |
| | Mixed | 28 | 0.90 | 4.91 |
| Age Class | 20-40 | 50 | 0.96 | 8.19 |
| | 41-60 | 27 | 1.56 | 13.05 |
| | 61-80 | 13 | 1.48 | 8.94 |
| | 81-100 | 29 | 0.72 | 3.01 |
| | 101+ | 14 | 1.30 | 5.66 |
| Density Class (Stems ha-1) | 250-500 | 4 | 1.13 | 3.92 |
| | 500-1000 | 13 | 1.03 | 4.59 |
| | 1001-1500 | 47 | 1.09 | 6.24 |
| | 1501-2000 | 12 | 1.95 | 19.66 |
| | 2001-2500 | 34 | 0.98 | 6.25 |
| | 2501-3000 | 23 | 1.00 | 9.88 |
| Understory Class | Minimal (1) | 34 | 0.91 | 4.06 |
| | Low (2) | 44 | 1.01 | 8.77 |
| | Moderate (3) | 25 | 1.17 | 7.34 |
| | Dense (4) | 15 | 0.99 | 4.87 |
| | Very Dense (5) | 15 | 1.94 | 17.59 |
| Tree Species | Balsam Fir | 17 | 1.31 | 14.80 |

| Factor | Factor Level | Number of Trees | Mean Absolute Error (cm) | Relative Mean Absolute Error (%) |
|---|---|---|---|---|
| Tree Species | Black Spruce | 35 | 0.92 | 8.99 |
| | Cedar | 5 | 0.80 | 3.39 |
| | Green Ash | 1 | 0.80 | 7.48 |
| | Jack Pine | 13 | 0.92 | 3.55 |
| | Red Maple | 4 | 2.02 | 9.21 |
| | Trembling Aspen | 46 | 1.15 | 5.72 |
| | White Birch | 5 | 1.26 | 6.30 |
| | White Spruce | 2 | 1.75 | 6.31 |
| | Yellow Birch | 5 | 1.32 | 12.74 |
| DBH Class (cm) | 7-10 | 30 | 1.08 | 13.58 |
| | 10.1-15 | 28 | 1.13 | 9.49 |
| | 15.1-20 | 23 | 1.02 | 5.95 |
| | 20.1-25 | 25 | 1.32 | 5.81 |
| | 25.1-30 | 17 | 0.82 | 3.02 |
| | 30.1-35 | 5 | 0.94 | 2.97 |
| | 35.1-40 | 3 | 1.13 | 3.00 |
| | 40.1-50 | 1 | 4.80 | 11.46 |

As highlighted in Figure 3.4, the data did not follow a normal distribution. The skewness was 3.17 with a Kurtosis value of 16.56, indicating a highly skewed dataset. To determine if any of the above factors had statistically significant impacts on the accuracy of DBH estimates (relative MAE; %), Kruskal-Wallis tests were used as this test accounts for the abnormal distribution of the results data (Xia 2020). Age class and density had large magnitudes of effect on the relative accuracy of the estimated DBH values for individual trees (Table 3.4). Understory classes had a moderate magnitude of

effect, while species class had a small effect on the accuracy of estimated DBH values. Age (0.17) and understory classes (0.13) had the greatest effect sizes when examined individually, as well as when examining pairwise interactions (0.23). Species class (0.01) had the smallest effect size on the relative accuracy of estimated DBH values.

**Table 3.4.** Kruskal-Wallis test results showing the statistical impact of individual stand- and site-level attributes and significant pairwise interactions on relative accuracy of DBH estimates.

| Factor(s) | Df | Test Statistic | *p*-Value | Effect Size | Magnitude Of Effect |
|---|---|---|---|---|---|
| Age Class | 4 | 25.95 | 3.24E-05 | 0.17 | Large |
| Density Class | 5 | 16.26 | 6.15E-04 | 0.09 | Moderate |
| Site Species Class | 2 | 2.78 | 0.25 | 0.01 | Small |
| Understory | 4 | 20.40 | 4.17E-04 | 0.13 | Moderate |
| DBH Class | 8 | 25.67 | 1.40E-03 | 0.14 | Moderate |
| Species | 9 | 12.67 | 0.18 | 0.03 | Small |
| Age Class * Density Class | 13 | 39.08 | 1.94E-04 | 0.22 | Large |
| Age Class * Site Species Class | 14 | 39.69 | 2.85E-04 | 0.22 | Large |
| Age Class * Understory | 12 | 39.34 | 9.23E-05 | 0.23 | Large |
| Density Class * Site Species Class | 13 | 37.86 | 3.04E-04 | 0.21 | Large |
| Density Class * Understory | 14 | 39.69 | 2.85E-04 | 0.22 | Large |
| Site Species Class * Understory | 9 | 25.76 | 2.23E-03 | 0.14 | Moderate |
| DBH Class * Age Class | 27 | 43.99 | 0.02 | 0.16 | Large |
| DBH Class * Density Class | 27 | 37.83 | 0.08 | 0.10 | Moderate |
| DBH Class * Site Species Class | 22 | 39.92 | 0.01 | 0.16 | Large |
| DBH Class * Understory | 29 | 55.36 | 6.43E-03 | 0.20 | Large |
| Age Class * Species | 22 | 45.91 | 2.03E-03 | 0.22 | Large |
| Density Class * Species | 22 | 36.26 | 0.03 | 0.13 | Moderate |
| Species * Understory | 21 | 49.49 | 4.29E-04 | 0.26 | Large |

Individual tree species had a small (0.03) effect on relative accuracy of estimated DBH values, whereas DBH size class had a moderate effect (0.14). For the individual site-level attributes that had significant effects on the accuracy of estimated DBH values (age, density, and understory classes), Dunn-Bonferroni post-hoc tests were conducted

to identify interactions between two values for a single variable with a significant impact on the accuracy of estimated DBH values (Table 3.5). Dunn-Bonferroni post-hoc testing identifies significant differences between different values of an independent variable that was found to have a significant impact on the dependent variable using a Kruskal-Wallis test (Dinno 2022).

**Table 3.5.** Dunn-Bonferroni post-hoc test results showing age classes, DBH categories, density categories, and understory classes with significant statistical differences.

| Factor | Group 1 | Group 2 | N1 | N2 | Statistic | *p*-Value |
|---|---|---|---|---|---|---|
| Age Class | 20-40 | 81-100 | 50 | 29 | -3.67 | 2.39E-04 |
| Age Class | 41-60 | 81-100 | 27 | 29 | -4.79 | 1.66E-06 |
| Age Class | 61-80 | 81-100 | 18 | 29 | -2.92 | 3.50E-03 |
| DBH Class | 7-10 cm | 25.1-30 cm | 30 | 17 | -3.71 | 2.09E-04 |
| DBH Class | 10.1-15 cm | 25.1-30 cm | 28 | 17 | -3.65 | 2.61E-04 |
| Density Class | 1001-1500 | 1501-2000 | 47 | 12 | 3.23 | 1.24E-03 |
| Density Class | 1501-2000 | 2001-2500 | 12 | 34 | -3.01 | 2.61E-03 |
| Density Class | 1501-2000 | 501-1000 | 12 | 13 | -3.4 | 6.66E-04 |
| Understory | Minimal (1) | Low (2) | 34 | 44 | 2.85 | 4.39E-03 |
| Understory | Minimal (1) | Very Dense (5) | 34 | 15 | 4.08 | 4.45E-05 |
| Understory | Dense (4) | Very Dense (5) | 15 | 15 | 3.17 | 1.50E-03 |

Below, Figure 3.5 shows a scatter plot of the estimated DBH (cm) for each individual tree (Coloured by site species class), plotted as a function of measured DBH (cm), with a line plotted showing a 1:1 relationship (i.e., $y = x$).

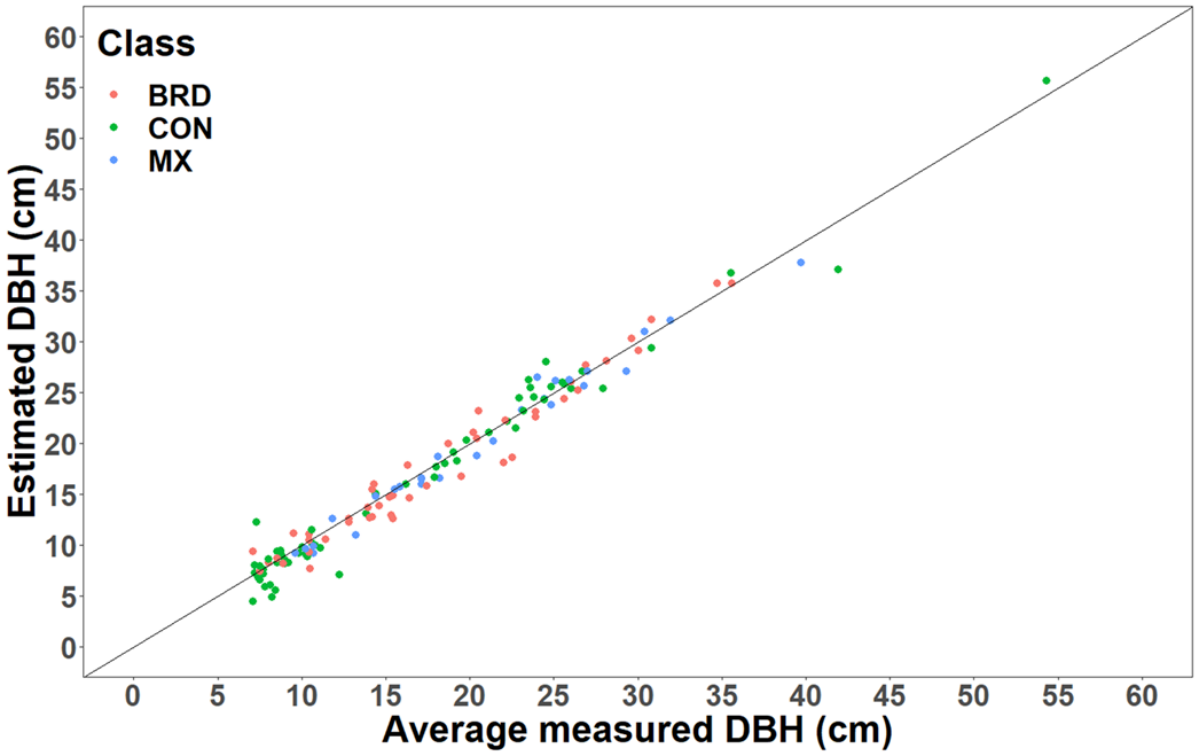


**Figure 3.5.** Histogram showing distribution of the number of trees as a function of the relative error values.

74 trees had estimated DBH values lower than the actual DBH values (55.6% of measured trees), with 53 estimated DBH values greater than the actual DBH values (39.9% of measured trees), with an additional 6 trees (4.5% of measured trees) having an estimated DBH equal to the actual DBH.

The pairwise interaction with the largest effect size was between individual tree species and understory classes (Table 3.4). Interactions between individual tree DBH size class and age class, species class, and understory class all had large effects (> 0.10) on the relative accuracy of individual tree DBH estimates. Overall, age class, individual tree DBH size class, and site understory classes had the largest effects on the accuracy of individual tree DBH estimates (Table 3.4).

### 3.3.3. Hypotheses

This study set out to investigate the effects of various site-level (Age Class, Species Class, Tree Density, Understory Density) and tree-level (Tree Species, Actual DBH) attributes on the relative accuracy of DBH values estimated using point cloud data acquired by an iPad Pro LiDAR scanner. It was found that all tested variables, with the exception of species class and individual tree species, had moderate to large magnitudes of effect on the relative accuracy of estimated DBH values (Tables 3.10-3.13). The secondary objective was to identify specific site conditions that facilitate or inhibit accurate estimation of DBH using the iPad Pro LiDAR scanner. While some trends were identified in the data, the results do not conclusively identify specific site conditions that facilitate or inhibit accurate estimation of DBH. Generally, sites with lower tree densities and less understory vegetation improved accuracy of DBH estimates, as did the measurement of larger trees (Table 3.3). In contrast, individual tree species, species composition, and stand age were not found to significantly affect the relative accuracy of estimated DBH values (Table 3.4).

It was hypothesised that DBH estimate accuracy would be lower in stands with significant leafy tissue or other obstructions at or around breast height (i.e., stands with high understory plant cover or stands with high tree densities). Our results showed that DBH estimates were most accurate in stands with minimal understory (Table 3.3). However, the results also show the understory class with the second most accurate estimates of DBH was the second-densest understory class. Understory class did have a moderate magnitude of effect on the relative accuracy of DBH estimates (Table 3.4). However, Dunn-Bonferroni post-hoc test for differences between levels of understory density suggested differences in the accuracies of estimated DBH values between these groups did not follow any trends (Table 3.5).

It was also hypothesised that the most accurate estimates of DBH would be achieved on sites with lower tree densities. Our results found that the lower three density classes (250-500 stems ha-1; 501-1000 stems ha-1; 1001-1500 stems ha-1) had more accurate estimates of DBH (Table 3.3). However, significant differences were observed between the 501-1000 and 1501-2000 stems ha-1 density classes; the 1001-1500 and 1501-2000 stems ha-1 classes; and, the 1501-2000 and 2001-2500 stems ha-1 classes. The most extreme density classes, 250-500 stems ha-1 and 2501-3000 stems ha-1, were not significantly different from one another or any of the other tested density classes. The lack of significant differences in estimate accuracy between the lowest and highest site density classes and the rest of the dataset suggests that site density alone is not sufficient to predict the accuracy of DBH estimates.

The final hypothesis suggested that the relative error of DBH estimates would decrease as tree size increased. With the exception of the sole tree in the 40 cm+ DBH class, relative error of DBH estimates decreased as tree size increased. Discarding the three size classes with 5 or fewer measured trees (30.1-35 cm; 35.1-40 cm; 40.1-50 cm), the 25.1-30 cm DBH class was the size class with the largest measured DBH values, and had the lowest relative error (Table 3.3). Dunn-Bonferroni post-hoc testing found significant differences between the 25.1-30 cm DBH class and both the 7-10 cm and 10.1-15 cm DBH classes (Table 3.5). This demonstrates that increases in actual DBH reduced the relative error of estimated DBH values in a statistically significant manner.

## 3.4. DISCUSSION

This study achieved an overall RMSE of 1.5 cm (8.6%) for DBH values estimated from iPad Pro LiDAR data for 15 sites in the boreal forest. This is a lower RMSE than those reported in several previous studies using the iPad Pro to estimate DBH, such as: an urban park (Slovakia), 2.8 cm (7.0%) and 5.2 cm (13.0%); a research forest (Austria), 3.1 cm (10.5%) and 6.3 cm (21.2%); Natural and plantation forests (Japan), 2.3 cm

(10.5%); and, a university campus (Türkiye), 2.3 cm (11.7%) (Gollob et al. 2021; Wang et al. 2021; Tatsumi et al. 2021; Gülci et al. 2023). A previous study using the same methodology as used in this study reported an RMSE of 1.1 cm (6.2%) for a plantation forest in Canada (Guenther et al. 2024).

Understory density was not considered when selecting sites for this study, as only site species composition and site age were known during the site selection period. As a result, the different combinations of understory density, site species class, and site age class were not evenly distributed, potentially causing bias in the results for the impact of understory density on the relative accuracy of estimated DBH values. Future research should incorporate multiple replicates of each combination of site species/age class to capture as much variation in understory density for that species/age class combination as possible.

Common causes of error identified in previous studies using the iPad Pro include IMU errors with the iPad Pro, as well as high proportions of misplaced points ('noise') in acquired point clouds (Gollob et al. 2021; Wang et al. 2021). IMU errors contribute to scanned features with low surface fidelities, especially when significant movement occurs during the acquisition of a given point cloud (Tavani et al. 2022; Corradetti et al. 2022). Other factors contributing to IMU errors include changes in walking speed, rapid movements, or turning the iPad during the course of a scan (Gollob et al. 2021; Guenther et al. 2024; Wang et al. 2021; Gülci et al. 2023). IMU errors were present in this study as well, with misaligned tree cross-sections encountered several times. The misalignments were manually corrected, although this introduced a potential cause of error. High levels of error in point location (±1 cm) in point clouds acquired with the iPad Pro LiDAR scanner have been found to cause trees to appear 'fuzzy' in the point clouds, which caused increased levels of error as tree size decree

sed (Gollob et al. 2021). This was also found in this study, with the relative accuracy of estimated DBH values lowest in the smallest DBH class and relative accuracy improving as actual DBH increased (Table 3.4).

Comparing the results of this study to previous studies using MLS or TLS in natural forests, RMSE values of 2.7 cm (10.8%; RANSAC method), 4.1 cm (16.3%; Circle Fit), and 6.8 cm (27.0%; Voxelization) were found in a study in a black pine (*Pinus nigra*) plantation forest in Italy (Chiappini et al. 2022). It was found that the accuracy of estimated DBH values was consistent for all sizes of tree recorded in the study. An MAE of 4.8 cm (25.9% RMSE) was achieved using MLS and an MAE of 5.0 cm (27.9% RMSE) using TLS to estimate DBH in a Ponderosa pine (*Pinus ponderosa*) forest in northern Arizona (Donager et al. 2021). An RMSE of 2.4 cm (5.6%) was achieved using TLS in managed Japanese cedar (*Cryptomeria japonica*) forests in Japan (Shimizu et al. 2022). Common causes of inaccuracy include occlusion of scanned trees from understory vegetation (Donager et al. 2021; Shimizu et al. 2022).

The results presented here support previous studies that found IMU errors, positional accuracy errors, and high levels of noise in point clouds to cause reduced accuracy of DBH values estimated using the iPad Pro LiDAR scanner. Factors identified as contributing to inaccuracies in previous studies using MLS or TLS to estimate DBH, such as high levels of understory vegetation or high site densities, were also found to reduce the accuracy of estimated DBH values with the iPad Pro. While tree size was found to impact the accuracy of DBH estimates both here and in previous studies using the iPad Pro LiDAR scanner, this factor did not impact the accuracy of DBH values estimated from TLS or MLS devices in previous studies, suggesting that this limiting factor is unique to the iPad Pro. The inclusion of additional site replicates for each combination of site age and site species class would further enhance future studies, increasing the size of the overall dataset as well as improving the diversity of

understory densities, individual tree species, and tree sizes present in each combination of site age and site species class.

## 3.5. CONCLUSIONS

Although there were no tested sites where all estimated DBH values fell within the acceptable margin of error (±1 cm based on OMNRF standards), this methodology estimated DBH values for all 133 scanned trees, with 78 of the estimated DBH values (59%) falling within the acceptable margin of error and 11 estimated DBH values (7%) within 0.1 cm of the validation value. It was found that site and understory density had statistically significant impacts on the accuracy of estimated DBH values, while site species class did not (Table 3.4). At the individual tree level, the actual DBH of a tree had a moderate effect on the accuracy of estimated DBH values, while individual tree species did not (Table 3.4).

Trends in the data suggested that increased density of both trees and understory vegetation on a given site would decrease the accuracy of estimated DBH values on the site, as hypothesized. Examining differences between the understory and site density classes with Dunn-Bonferroni post-hoc testing, it was found that these factors had significant impacts on the relative accuracy of estimated DBH values. However, the differences between different classes of these variables did not present a consistent or continuous relationship, with no strong trends present. Increases in actual tree size led to increases in the relative accuracy of estimated DBH values. Dunn-Bonferroni post-hoc testing showed that the relative accuracy of estimated DBH values improved as measured tree size increased, supporting this hypothesis.

The results of this study suggest that the significant impacts of site understory, actual tree size, age class, and density will impact the accuracy of estimated DBH values in future studies using the iPad Pro to estimate DBH, and must be addressed and characterized in future studies to better contextualize results in a broader context. At

this point in time, the persistent issues with the iPad Pro IMU and positional accuracy errors limit accuracy of DBH estimates attainable with the iPad Pro LiDAR scanner in natural boreal forests. Additionally, the use of iPad Pro LiDAR for forest inventory is limited by an inability to perform well in unfavorable weather conditions, such as rain, fog, or wind, limiting the operational feasibility of this method at the industry scale. The iPad Pro shows promise, meeting accuracy specifications for 59% of the scanned trees across 15 sites representing a range of site conditions in boreal forests. However, current limitations prevent this device from being operationalizable in the boreal forest to replace manual mensuration of DBH for forest inventories.

# CHAPTER 4: CONCLUSIONS AND RECOMMENDATIONS FOR FUTURE RESEARCH

In Chapter 2, the use of a circular scanning pattern for point cloud acquisition, coupled with the application of a combination of circle-fitting and ellipse-fitting formulas to a single 4 cm cross-section of a tree stem was found to produce the most accurate estimates of DBH. The factors with the greatest effects on the accuracy of estimated DBH values were scanning pattern and curve-fitting formula. Cross-section size and cross-section count had small effects on the accuracy of estimated DBH values. However, the circular scanning pattern with combined curve-fitting formula produced the most accurate estimates of DBH using a single 4 cm cross-section. Factors contributing to the error in the identified optimal method included the presence of noise (points in the acquired point cloud that are not in the correct location as the feature they represent), IMU drift, and rotational errors. The curve-fitting formulas used are optimized for datasets containing at least 400 points representing 50% of the circumference of the curve to be fitted, which was not the case with tree stems extracted from point clouds acquired with either the figure-8 or transect scanning patterns.

In the case study, Overall, an RMSE of 1.5 cm (8.6%) was achieved, with 78 (59%) of the estimated DBH values within an acceptable margin of error (±1 cm) of the validation values based on OMNRF standards. This level of accuracy is insufficient for use in forest inventories, and until DBH can be consistently estimated within the acceptable margin of error for a significantly greater percentage of trees, this methodology will be unsuitable for use in FRIs. Stand age had the greatest effect size on estimated DBH values, followed by actual DBH, understory density, and stand density. Tree species or stand species class did not have significant effects on the accuracy of estimated DBH values. While some trends were identified in the results, statistical analyses showed these were inconclusive. Generally, it was found that estimated DBH

values were more accurate on sites with lower tree densities as well as sites with less understory vegetation. An alternative remote sensing methods, especially, RADAR, are capable of scanning 'through' obstacles such as understory vegetation, and mapping features beyond the obstacles, data. Accuracy of estimated DBH values also improved as the size of the tree being scanned increased to the 30.1-35 cm size class, with increased error observed in subsequent size classes. However, Dunn-Bonferroni post-hoc testing showed that none of these variables alone were sufficient to predict the accuracy of estimated DBH values.

As the case study described in Chapter 3 was limited to a small number of sites, the impacts of the tested stand-level and tree-level factors cannot be conclusively identified from this limited dataset. Therefore, a future study that tests multiple replicates of sites to capture the range of site densities and understory densities within each combination of age class and species class is necessary. Additionally, future research should compare the accuracy of DBH values estimated from the iPad Pro and traditional MLS/TLS using the same processing methodology for a range of boreal forest stand conditions. This would allow direct comparisons between the accuracy of the iPad Pro and traditional MLS/TLS in natural boreal forests to be made. While DBH was estimated in a broad range of natural boreal forest stand conditions, 41% of trees in the case study failed to meet OMNRF accuracy specifications for DBH. Future research should attempt to improve data acquisition and processing methodologies to improve the portion of estimated DBH values meeting minimum standards of measurement accuracy.

Another key factor to be considered in future studies is the efficiency of using the iPad Pro LiDAR scanner to estimate DBH. This study did not record the speed of data acquisition in the field with either manual methods or with the iPad Pro. It was observed that field crews using manual methods to measure DBH, as well as recording tree heights, species, and canopies, were able to complete a 400m$^2$ VSN plot in less time

than it took to acquire LiDAR data with the iPad Pro. While the literature hypothesizes that the use of LiDAR devices to estimate DBH will improve the speed of forest inventories relative to manual methods, the opposite was observed in this study. Quantitative data should be collected to validate this observation. Additionally, the acquired point clouds still need to synced to cloud services and processed to estimate DBH after returning from the field, while the manually measured data does not require additional man-hours. Until point cloud acquisition with the iPad Pro can be completed faster than manual mensuration of DBH, the iPad Pro is entirely impracticable. Furthermore, the iPad Pro LiDAR scanner currently uses only near infrared wavelength. Incorporating additional wavelengths (green band) as in aerial LiDAR would improve the accuracy of features scanned.

As noted in the Introduction (Chapter 1), DBH is one of many attributes measured for forest inventories. An overarching question addressed in this thesis was whether the iPad Pro 4$^{th}$ Generation TLS device can be used to reliably estimate DBH, a forest attribute common in forest inventories. If so, its use might offer an improvement in efficiency and a reduction in operating costs for the undertaker of the inventory, relative to TLS or manual measurements. Current results show that DBH cannot be estimated with an acceptable level of accuracy. Additionally, future studies must also determine if additional tree and stand attributes (e.g., tree species, tree height, stand density, etc.) critical to creating new eFRIs can be accurately estimated from iPad Pro LiDAR before the device can be considered as a viable alternative method of data collection in forest inventories. The current maximum range of the iPad Pro LiDAR scanner is only 5m, rendering the device incapable of capturing point clouds that would allow estimation of attributes such as tree height (commonly greater than 20m in mature boreal stands.

## LITERATURE CITED


Aijazi, A. K., Checchin, P., Malaterre, L., & Trassoudaine, L. 2017. Automatic Detection and Parameter Estimation of Trees for Forest Inventory Applications Using 3D Terrestrial LiDAR. *Remote Sensing*, *9*(9), Article 9. https://doi.org/10.3390/rs9090946

Apple. 2020. *Apple unveils new iPad Pro with LiDAR Scanner and trackpad support in iPadOS*. Apple Newsroom. https://www.apple.com/newsroom/2020/03/apple-unveils-new-ipad-pro-with-lidar-scanner-and-trackpad-support-in-ipados/

Balenović, I., Liang, X., Jurjević, L., Hyyppä, J., Seletković, A., & Kukko, A. 2021. Hand-Held Personal Laser Scanning: Current Status and Perspectives for Forest Inventory Application. *Croatian Journal of Forest Engineering*, *42*(1), Article 1. https://doi.org/10.5552/crojfe.2021.858

Bauwens, S., Bartholomeus, H., Calders, K., & Lejeune, P. 2016. Forest Inventory with Terrestrial LiDAR: A Comparison of Static and Hand-Held Mobile Laser Scanning. *Forests*, *7*(6), Article 6. https://doi.org/10.3390/f7060127

Bilyk, A., Pulkki, R., Shahi, C., & Larocque, G. R. 2021. Development of the Ontario Forest Resources Inventory: a historical review. *Canadian Journal of Forest Research*, *51*(2), 198–209. https://doi.org/10.1139/cjfr-2020-0234

Bivand, R., Keitt, T., Rowlingson, B., Pebesma, E., Sumner, M., Hijmans, R., Baston, D., Rouault, E., Warmerdam, F., Ooms, J., & Rundel, C. 2023. *rgdal: Bindings for the 'Geospatial' Data Abstraction Library* (1.6-7). https://cloud.r-project.org/web/packages/rgdal/index.html

Blanco, A. C., Tamondong, A. M., Perez, A. M. C., Ang, M. R. C. O., & Paringit, E. C. 2015. The PHIL-LiDAR 2 Program: National Forest Resource Inventory of the Phillipines using LiDAR and other Remotely Sensed Data. *The International Archives of the Photogrammetry, Remote*

*Sensing and Spatial Information Sciences*, *XL-7/W3*, 1123–1127. https://doi.org/10.5194/isprsarchives-XL-7-W3-1123-2015

Calders, K., Adams, J., Armston, J., Bartholomeus, H., Bauwens, S., Bentley, L. P., Chave, J., Danson, F. M., Demol, M., Disney, M., Gaulton, R., Krishna Moorthy, S. M., Levick, S. R., Saarinen, N., Schaaf, C., Stovall, A., Terryn, L., Wilkes, P., & Verbeeck, H. 2020. Terrestrial laser scanning in forest ecology: Expanding the horizon. *Remote Sensing of Environment*, *251*, 112102. https://doi.org/10.1016/j.rse.2020.112102

Castel, C., D'Hoedt, M. 2022. *Automated forest inventory using the iPad Pro LiDAR scanner* [Masters]. Ecole Polytechnique de Louvain, Universite Cathiolique de Louvain.

Chen, Q., Gao, T., Zhu, J., Wu, F., Li, X., Lu, D., & Yu, F. 2022. Individual Tree Segmentation and Tree Height Estimation Using Leaf-Off and Leaf-On UAV-LiDAR Data in Dense Deciduous Forests. *Remote Sensing*, *14*(12), Article 12. https://doi.org/10.3390/rs14122787

Chernov, N. 2022a. *Circle Fit (Pratt method)* (1.0.0) [MATLAB; Windows]. MathWorks. https://www.mathworks.com/matlabcentral/fileexchange/22643-circle-fit-pratt-method

Chernov, N. 2022b. *Circle Fit (Taubin method)* (1.0.0) [MATLAB; Windows]. MathWorks. https://www.mathworks.com/matlabcentral/fileexchange/22678-circle-fit-taubin-method

Chernov, N. 2022c. *Ellipse Fit (Direct method)* (1.1.0.0) [MATLAB; Windows]. MathWorks. https://www.mathworks.com/matlabcentral/fileexchange/22684-ellipse-fit-direct-method

Chernov, N., Gama, J. 2015. *conicfit: Algorithms for Fitting Circles, Ellipses and Conics* (1.0.4) [R].

Chernov, N., Lesort, C. 2005. Least squares Fitting of Circles. *Journal of Mathematical Imaging and Vision*, *23*, 239–252.

Chiappini, S., Pierdicca, R., Malandra, F., Tonelli, E., Malinverni, E. S., Urbinati, C., & Vitali, A. 2022. Comparing Mobile Laser Scanner and manual measurements for dendrometric variables

estimation in a black pine (Pinus nigra Arn.) plantation. *Computers and Electronics in Agriculture*, *198*, 107069. https://doi.org/10.1016/j.compag.2022.107069

Corradetti, A., Seers, T., Mercuri, M., Calligaris, C., Busetti, A., & Zini, L. 2022. Benchmarking Different SfM-MVS Photogrammetric and iOS LiDAR Acquisition Methods for the Digital Preservation of a Short-Lived Excavation: A Case Study from an Area of Sinkhole Related Subsidence. *Remote Sensing*, *14*(20), Article 20. https://doi.org/10.3390/rs14205187

Côté, J.-F., Fournier, R. A., & Egli, R. 2011. An architectural model of trees to estimate forest structural attributes using terrestrial LiDAR. *Environmental Modelling & Software*, *26*(6), 761–777. https://doi.org/10.1016/j.envsoft.2010.12.008

Dassot, M., Constant, T., & Fournier, M. 2011. The use of terrestrial LiDAR technology in forest science: application fields, benefits and challenges. *Annals of Forest Science*, *68*(5), Article 5. https://doi.org/10.1007/s13595-011-0102-2

Dinno, A. 2022. *Package 'dunn.test'*. https://cran.r-project.org/web/packages/dunn.test/dunn.test.pdf

Donager, J. J., Sánchez Meador, A. J., & Blackburn, R. C. 2021. Adjudicating Perspectives on Forest Structure: How Do Airborne, Terrestrial, and Mobile Lidar-Derived Estimates Compare? *Remote Sensing*, *13*(12), Article 12. https://doi.org/10.3390/rs13122297

ESRI. 2023. *ArcGIS Pro* (3.10) [C++; Windows]. ESRI, Redlands, CA, USA. esri.com/en-us/arcgis/products/arcgis-pro/overview

Girardeau-Montaut, D. 2022. *CloudCompare - Open Source project* (2.12.4 Kyiv) [C++; Windows]. CloudCompare. https://www.cloudcompare.org/

Gollob, C., Ritter, T., Kraßnitzer, R., Tockner, A., & Nothdurft, A. 2021. Measurement of Forest Inventory Parameters with Apple iPad Pro and Integrated LiDAR Technology. *Remote Sensing*, *13*(16), Article 16. https://doi.org/10.3390/rs13163129

Guenther, M., Heenkenda, M. K., Leblon, B., Morris, D., & Freeburn, J. T. 2024. Estimating Tree Diameter at Breast Height (DBH) using iPad Pro Light Detection and Ranging (LiDAR) Sensor in Boreal Forests. *Canadian Journal of Remote Sensing*, *50*(1), no. 2295470. https://doi.org/10.1080/07038992.2023.2295470

Gülci, S., Yurtseven, H., Akay, A. O., & Akgul, M. 2023. Measuring tree diameter using a LiDAR-equipped smartphone: a comparison of smartphone- and caliper-based DBH. *Environmental Monitoring and Assessment*, *195*(6), 678. https://doi.org/10.1007/s10661-023-11366-8

Hopkinson, C., Chasmer, L., Young-Pow, C., & Treitz, P. 2004. Assessing forest metrics with a ground-based scanning lidar. *Canadian Journal of Forest Research*, *34*(3), 573–583. https://doi.org/10.1139/x03-225

Hunčaga, M., Chudá, J., Tomaštík, J., Slámová, M., Koreň, M., & Chudý, F. 2020. The Comparison of Stem Curve Accuracy Determined from Point Clouds Acquired by Different Terrestrial Remote Sensing Methods. *Remote Sensing*, *12*(17), Article 17. https://doi.org/10.3390/rs12172739

Hyyppä, E., Hyyppä, J., Hakala, T., Kukko, A., Wulder, M. A., White, J. C., Pyörälä, J., Yu, X., Wang, Y., Virtanen, J.-P., Pohjavirta, O., Liang, X., Holopainen, M., & Kaartinen, H. 2020. Under-canopy UAV laser scanning for accurate forest field measurements. *ISPRS Journal of Photogrammetry and Remote Sensing*, *164*, 41–60. https://doi.org/10.1016/j.isprsjprs.2020.03.021

Lee, J. B., Jung, J. H., & Kim, H. J. 2020. Segmentation of Seabed Points from Airborne Bathymetric LiDAR Point Clouds Using Cloth Simulation Filtering Algorithm. *Journal of the Korean Society of Surveying, Geodesy, Photogrammetry and Cartography*, *38*(1), 1–9. https://doi.org/10.7848/ksgpc.2020.38.1.1

Liang, X., Hyyppä, J., Kaartinen, H., Lehtomäki, M., Pyörälä, J., Pfeifer, N., Holopainen, M., Brolly, G., Francesco, P., Hackenberg, J., Huang, H., Jo, H.-W., Katoh, M., Liu, L., Mokroš, M., Morel, J., Olofsson, K., Poveda-Lopez, J., Trochta, J., … Wang, Y. 2018. International benchmarking of terrestrial laser scanning approaches for forest inventories. *ISPRS Journal of Photogrammetry and Remote Sensing*, *144*, 137–179. https://doi.org/10.1016/j.isprsjprs.2018.06.021

Liu, G., Wang, J., Dong, P., Chen, Y., & Liu, Z. 2018. Estimating Individual Tree Height and Diameter at Breast Height (DBH) from Terrestrial Laser Scanning (TLS) Data at Plot Level. *Forests*, *9*(7), Article 7. https://doi.org/10.3390/f9070398

Liu, L., Zhang, A., Xiao, S., Hu, S., He, N., Pang, H., Zhang, X., & Yang, S. 2021. Single Tree Segmentation and Diameter at Breast Height Estimation With Mobile LiDAR. *IEEE Access*, *9*, 24314–24325. https://doi.org/10.1109/ACCESS.2021.3056877

Lovell, J. L., Jupp, D. L. B., Culvenor, D. S., & Coops, N. C. 2003. Using airborne and ground-based ranging lidar to measure canopy structure in Australian forests. *Canadian Journal of Remote Sensing*, *29*(5), 607–622. https://doi.org/10.5589/m03-026

Luetzenburg, G., Kroon, A., & Bjørk, A. A. 2021. Evaluation of the Apple iPhone 12 Pro LiDAR for an Application in Geosciences. *Scientific Reports*, *11*(1), Article 1. https://doi.org/10.1038/s41598-021-01763-9

McClain, K. M., Morris, D. M., Hills, S. C., & Buse, L. J. 1994. The effects of initial spacing on growth and crown development for planted northern conifers: 37-year results. *The Forestry Chronicle*, *70*(2), 174–182. https://doi.org/10.5558/tfc70174-2

Moler, C., Little, J. N., Bangert, S., & Johnson, S. C. 2022. *MATLAB - MathWorks* (Version R2022b) [C; Windows]. MathWorks, Natick, MA, USA. https://www.mathworks.com/products/matlab.html

Moran, L. A., & Williams, R. A. 2002. Comparison of Three Dendrometers in Measuring Diameter at Breast Height. *Northern Journal of Applied Forestry*, *19*, 28–33.

Müller, A., Olschewski, R., Unterberger, C., & Knoke, T. 2020. The valuation of forest ecosystem services as a tool for management planning – A choice experiment | Elsevier Enhanced Reader. *Journal of Environmental Management*, *271*, 13. https://doi.org/10.1016/j.jenvman.2020.111008

Ontario Ministry of Natural Resources and Forestry. 2015. *Forest Management Guide to Silviculture in the Great Lakes-St. Lawrence and Boreal Forests of Ontario*. Queen's Printer for Ontario.

Ontario Ministry of Natural Resources and Forestry. 2021. *Vegetation Sampling Network Protocol: Technical specifications for field plots.* (2.0). Ontario Ministry of Natural Resources and Forestry, Science and Research Branch.

Pfeifer, N., & Winterhalder, D. 2004. Modelling of Tree Cross Sections from Terrestrial Laser Scanning Data with Free-Form Curves. *International Archives of Photogrammetry, Remote Sensing, and Spatial Information Sciences*, *36*(8), 76–81.

Pratt, V. 1987. Direct least-squares fitting of algebraic surfaces | Proceedings of the 14th annual conference on Computer graphics and interactive techniques. *Computer Graphics*, *21*(4), 145–152. https://doi.org/ACM-0-89791-227-6/87/007/0145

Shimizu, K., Nishizono, T., Kitahara, F., Fukumoto, K., & Saito, H. 2022. Integrating terrestrial laser scanning and unmanned aerial vehicle photogrammetry to estimate individual tree attributes in managed coniferous forests in Japan. *International Journal of Applied Earth Observation and Geoinformation*, *106*, 102658. https://doi.org/10.1016/j.jag.2021.102658

Szpak, D. Z. L. 2016. *Guaranteed Ellipse Fitting with a Confidence Region and an Uncertainty Measure for Centre, Axes and Orientation* [Matlab].

https://github.com/zygmuntszpak/guaranteed-ellipse-fitting-with-a-confidence-region-and-an-uncertainty-measure (Original work published 2015)

Szpak, Z. L., Chojnacki, W., & van den Hengel, A. 2015. Guaranteed Ellipse Fitting with a Confidence Region and an Uncertainty Measure for Centre, Axes, and Orientation. *Journal of Mathematical Imaging and Vision*, *52*(2), 173–199. https://doi.org/10.1007/s10851-014-0536-x

Tatsumi, S., Yamaguchi, K., & Furuya, N. 2021. ForestScanner: A mobile application for measuring and mapping trees with LiDAR-equipped iPhone and iPad. *Methods in Ecology and Evolution*, *0*(0), 7. https://doi.org/10.1111/2041-210X.13900

Taubin, G. 1991. Estimation of planar curves, surfaces, and nonplanar space curves defined by implicit equations with applications to edge and range image segmentation. *IEEE Transactions on Pattern Analysis and Machine Intelligence*, *13*(11), 1115–1138. https://doi.org/10.1109/34.103273

Tavani, S., Billi, A., Corradetti, A., Mercuri, M., Bosman, A., Cuffaro, M., Seers, T., & Carminati, E. 2022. Smartphone assisted fieldwork: Towards the digital transition of geoscience fieldwork using LiDAR-equipped iPhones. *Earth-Science Reviews*, *227*, 103969. https://doi.org/10.1016/j.earscirev.2022.103969

Turner, K. J. 1974. *Computer Perception of Curved Objects Using a Television Camera* [Ph. D., The University of Edinburgh]. https://era.ed.ac.uk/handle/1842/8129

Veesus. 2022. *ZAPPCHA: Mobile LiDAR Scanner* (5.6) [Swift; iOS]. Veesus. https://zappcha.com/

Wang, C., Ji, M., Wang, J., Wen, W., Li, T., & Sun, Y. 2019. An Improved DBSCAN Method for LiDAR Data Segmentation with Automatic Eps Estimation. *Sensors (Basel, Switzerland)*, *19*(1), 172. https://doi.org/10.3390/s19010172

Wang, F., Heenkenda, M. K., & Freeburn, J. T. 2022. Estimating tree Diameter at Breast Height (DBH) using an iPad Pro LiDAR sensor. *Remote Sensing Letters*, *13*(6), 568–578. https://doi.org/10.1080/2150704X.2022.2051635

Wang, X., Singh, A., Pervysheva, Y., Lamatungga, K. E., Murtinová, V., Mukarram, M., Zhu, Q., Song, K., Surový, P., & Mokroš, M. 2021. Evaluation of iPad Pro 2020 LiDAR for Estimating Tree Diameters in Urban Forest. *ISPRS Annals of the Photogrammetry, Remote Sensing and Spatial Information Sciences*, *VIII-4/W1-2021*, 105–110. https://doi.org/10.5194/isprs-annals-VIII-4-W1-2021-105-2021

White, J. C., Coops, N. C., Wulder, M. A., Vastaranta, M., Hilker, T., & Tompalski, P. 2016. Remote Sensing Technologies for Enhancing Forest Inventories: A Review. *Canadian Journal of Remote Sensing*, *42*(5), 619–641. https://doi.org/10.1080/07038992.2016.1207484

Woods, M., Pitt, D., Penner, M., Lim, K., Nesbitt, D., Etheridge, D., & Treitz, P. 2011. Operational implementation of a LiDAR inventory in Boreal Ontario. *The Forestry Chronicle*, *87*(04), 512–528. https://doi.org/10.5558/tfc2011-050

Xia, Y. 2020. Chapter Eleven - Correlation and association analyses in microbiome study integrating multiomics in health and disease. In J. Sun (Ed.), *Progress in Molecular Biology and Translational Science* (Vol. 171, pp. 309–491). Academic Press. https://doi.org/10.1016/bs.pmbts.2020.04.003

Yang, A., Wu, Z., Yang, F., Su, D., Ma, Y., Zhao, D., & Qi, C. 2020. Filtering of airborne LiDAR bathymetry based on bidirectional cloth simulation. *ISPRS Journal of Photogrammetry and Remote Sensing*, *163*, 49–61. https://doi.org/10.1016/j.isprsjprs.2020.03.004

Yu, D., He, L., Ye, F., Jiang, L., Zhang, C., Fang, Z., & Liang, Z. 2022. Unsupervised ground filtering of airborne-based 3D meshes using a robust cloth simulation. *International Journal of*

*Applied Earth Observation and Geoinformation*, *111*, 102830. https://doi.org/10.1016/j.jag.2022.102830

Zhang, W., Qi, J., Wan, P., Wang, H., Xie, D., Wang, X., & Yan, G. 2016. An Easy-to-Use Airborne LiDAR Data Filtering Method Based on Cloth Simulation. *Remote Sensing*, *8*(6), Article 6. https://doi.org/10.3390/rs8060501

## Curriculum Vitae

**Candidate's Full Name:** Matthew Guenther

**Universities Attended:**

- Lakehead University (Thunder Bay, ON)
    - (Honours Bachelor of Science: Forestry)
    - Attended: Fall 2018 – Spring 2022
- Lakehead University (Thunder Bay, ON)
    - (Master of Science: Forestry. Pursuing.)
    - Attended: Fall 2022 – Spring 2024

**Publications:**

- Guenther, M.; Heenkenda, M.K.; Leblon, B.; Morris, D.; Freeburn, J. Estimating Tree Diameter at Breast Height (DBH) Using iPad Pro LiDAR Sensor in Boreal Forests. Canadian Journal of Remote Sensing 2024, 50(1), 2295470, doi:10.1080/07038992.2023.2295470.
- Guenther, M.; Heenkenda, M.K.; Morris, D.; Leblon, B. Tree Diameter at Breast Height (DBH) Estimation Using an iPad Pro LiDAR Scanner: A Case Study in Boreal Forests, Ontario, Canada. Forests 2024, 15, 214, doi:10.3390/f15010214.

**Conference Presentations:**

- Guenther, M.; Heenkenda, M.K.; Morris, D.; Leblon, B. Best Practices: Estimating Tree Diameter at Breast Height with iPad Pro LiDAR in Boreal Forests. Oral presentation at the 44th Canadian Symposium on Remote Sensing: Monitoring Our Dynamic Environment; Remote Sensing for a Sustainable Future. Yellowknife, YT, Canada. June 19-22, 2023.